Part I: Hydrological properties within the eastern Indonesian throughflow region during the INDOMIX experiment

Agus Atmadipoera, Ariane Koch-Larrouy, Gurvan Madec, Jacques Grelet, François Baurand, Indra Jaya, Isabelle Dadou

Deep Sea Research Part I: Oceanographic Research Papers
April 2022, Volume 182 Pages 103735 (22p.)
https://doi.org/10.1016/j.dsr.2022.103735
https://archimer.ifremer.fr/doc/00752/86444/

Part I: Hydrological properties within the eastern Indonesian throughflow region during the INDOMIX experiment

Atmadipoera Agus S. [1, *], Koch-Larrouy Ariane [2, 3], Madec Gurvan [4], Grelet Jacques [5], Baurand Francois [5], Jaya Indra [1], Dadou Isabelle [2]

[1] IPB University, Bogor, Indonesia
[2] LEGOS, University of Toulouse, UMR5566 CNES-IRD-CNRS-UPS, France
[3] MERCATOR-OCEAN, Toulouse, France
[4] LOCEAN, Paris, France
[5] IMAGO IRD Brest, France

* Corresponding author : Agus S. Atmadipoera, email address : atmadipoera_itk@apps.ipb.ac.id

Abstract :

The Indonesian Mixing (INDOMIX) cruise of July 2010, resolves the Pacific Ocean water masses spreading from the Halmahera Sea through the Seram Sea, Manipa Strait, Banda Sea, to the Ombai Strait, and along the southern margin of Lesser Sunda Arc across the northern Savu Sea, Sumba Strait, and south of Lombok Strait. This paper focuses on the characteristics and stratification of the water masses, along this path and Part II of this study discusses the biogeochemical aspects. Two companion papers on quantification of turbulent mixing have been published elsewhere. We find: a) A marked transformation of South Pacific (SP) thermocline water within a sharp salinity front between the Halmahera Seram Seas. Tidally induced vertical mixing is the main process weakening the SP stratification, as suggested by a simple 1-dimensional diffusion model forced by vertical diffusivity of INDOMIX vertical microstructure profiler dataset. The transformation of SP water by vertical mixing can occur after 3 days, which is in good agreement with previously reported water mass residence times. Lateral advection plays a minor role; b) Interleaving salinity structure within the thermocline of the central Halmahera Sea and two deeper inflow channels. The interleaving salinity features within the central Halmahera Sea thermocline occurs where vertical diffusivity is relatively weak, compared to the vertical mixing at entry/exit portal that removes the interleaving salinity features. Two deeper inflow channels (about 950 m and 740 m depth) in the entry portal of the Halmahera Sea are mapped from the multi-beam echo sounder measurement, where both channels allow the renewal of SP thermocline water and salinity interleaving processes; c) Northward flow of thermocline water (100–200 m depth) in the Manipa Strait that injects Banda homogeneous salinity water into Seram Sea that erode Halmahera salty water via strong diapycnal mixing; d) Cyclonic upper layer circulation in Banda where eastward (westward) flow occurs in the northern (southern) Banda, confirmed by recent modeling study; and e) Relative salty Indian Ocean intermediate water flowing along southern margin of the Lesser Sunda Arc, within the South Java Undercurrent. Two distinct upper thermocline water, due to different source of Indonesian Throughflow (ITF) water, are found in the Banda Sea: fresher and colder water contrasting to saltier and warmer water that converge in this confluence region. Beneath it, Banda intermediate homogeneous salinity water and low dissolved oxygen water is dominant.

Highlights

► The INDOMIX cruise dataset resolve the Pacific Ocean water masses spreading in the eastern Indonesian Throughflow region. ► Strong transformation of South Pacific (SP) thermocline water front is found between the Halmahera and Seram seas. ► Tidally induced vertical mixing is the main processs of extinction of SP stratification, as suggested by the diffusion model. ► Interleaving salinity structure in the central Halmahera Sea is related to a weak vertical diffusivity and renewal SP water. ► North Indian Intermediate Water flowing along southern margin of the Lesser Sunda Arc within the South Java Undercurrent.

Keywords : INDOMIX cruise, Hydrographic measurement, ITF water masses, Eastern Indonesian archipelago, North and South Pacific water, North Indian intermediate water, Tidally induced vertical mixing

1. INTRODUCTION

The deep eastern Indonesian Archipelago mostly facilitates the inter-basin transfer of heat and freshwater flux from the Pacific to the Indian Oceans, known as the Indonesian Throughflow (ITF). The ITF is the sole prominent branch of returned warm surface flow at low latitudes in global thermohaline circulation. This transfer has significant effects on the heat and freshwater budget of the two basins, which in turn, impacts the variability of coupled ocean-atmosphere fluxes on larger spatial scales (Godfrey, 1996; Gordon, 1986; Gordon and Fine, 1996; Meyers, 1996; Wang et al., 2009).

The distribution of water masses within the eastern Indonesian Archipelago originating from the Pacific has been widely documented from both observation and modeling studies within the main ITF route and its exit straits (Atmadipoera et al., 2009; Gordon, 2005; Gordon and Fine, 1996; Ilahude and Gordon, 1996; Van Aken et al., 1988; Wyrtki, 1961). Previous work indicates that the ITF water masses are characterized by a very strong transformation between the inflow and outflow e.g., (Atmadipoera et al., 2009; Gordon, 2005; Ilahude and Gordon, 1996). The western route, fed by the southward Mindanao Current, transports water from the North Pacific into the Indonesian seas; only the shallower part passes through the Dewakang Strait at depths above 680 m (Fig.1). This water is formed by North Pacific Subtropical Waters (NPSW), characterized by a salinity maximum down to a depth of approximately 150 m, and North Pacific Intermediate Water (NPIW) with a salinity minimum (34.2 psu) at deeper thermocline depths. The ITF eastern route, fed by the New Guinea Under Current, transports saltier (35.4 psu) water from the South Pacific, from which only the lower parts of the thermocline and deeper layer enter the Indonesian basins. Their salinity signature is visible at lower thermocline depths, in contrast with less saline from

the Makassar Strait (Atmadipoera et al., 2009; Gordon, 2005; Ilahude and Gordon, 1996). Gradually, these salinity extremes are eroded, with major differences in each basin. The salinity maximum of the NPSW from 35.0 to 34.8–34.4 psu enters Indonesian seas into the Makassar Strait (Fig. 1). Meanwhile, the salinity minimum of NPIW increases from 34.2 to 34.4 psu from the northern entrance to the Makassar Strait (Ilahude and Gordon, 1996). Very fresh surface water from the Java Sea has a very low salinity. This near-surface water is advected by eastward monsoon currents with salty thermocline ITF in the Makassar Strait. As a result of strong diapycnal mixing along the Flores Sea pathway, this very fresh surface water penetrates down to the thermocline depth. As a result, the ITF water appears to be a fresh near-surface and thermocline water (<34.5 psu) in the Banda Sea and the outflow straits (Lombok, Ombai, Timor), as well as downstream in the eastern Indian Ocean (Atmadipoera et al., 2009; Fieux et al., 2005, 1994; Molcard et al., 2001, 1996; Wijffels et al., 2002).

The Makassar inflow proceeds through the Banda basin via the Flores Sea, where a high-salinity of 34.6 psu from NPSW and a salinity minimum of 34.45 psu from NPIW are found in the thermocline and at intermediate depths respectively (Gordon and Fine, 1996; Ilahude and Gordon, 1996; Wyrtki, 1961). Similarly, for the eastern route passing by the Maluku and Halmahera Seas (Fig. 1), the salinity maximum of South Pacific Subtropical water (SPSW) decreases from 35.5 psu in the Pacific compared to 34.8–35.0 psu in the interior seas (Atmadipoera et al., 2009; Ilahude and Gordon, 1996). In the Banda Sea, where the two routes converge, and in the Timor passage, salinity extremes are not recorded; instead, a nearly homogeneous water with a salinity of 34.6 psu is found below the 20 °C isotherm (Cresswell et al., 1993; Fieux et al., 1994). In the Indian Ocean, the Indonesian thermocline water is exported westward by the South Equatorial Current and creates a cold and fresh tongue relative

to the Indian water, spreading zonally between latitudes of 10 °S and 20 °S (Talley and Sprintall, 2005; Wijffels et al., 2002).

The International Nusantara Stratification and Transport (INSTANT) program provided three consecutive years (2004–2006) of ITF transport, heat, and mass fluxes, measured simultaneously in the inflow and outflow straits. The sum of mean ITF inflows via Makassar and Lifamatola is 13 Sv (Gordon et al., 2010, 2008; van Aken et al., 2009), and the mean outflow via Lombok, Ombai, and Timor is 15 Sv (Sprintall et al., 2009). These measurements indicate a discrepancy of about 2 Sv between the inflow and outflow, which likely results from the uncertainties of the calculation method and from the unmeasured transport from the shallow Karimata Strait (entrance of the Java Sea Water) and Halmahera Sea (Gordon et al., 2010). For example, in the Karimata Strait throughflow, Fang et al. (2010) found a southward transport volume of 3.6 Sv during the northwest monsoon (January and February 2008), with possible large seasonal variations and flow reversal during the southeast monsoon.

In the Halmahera Sea, Luick and Cresswell (2001) reported a mean transport inflow of about 1.5 Sv from current measurements during one year (mid-1993 to mid-1994). The inflow portal through the Halmahera Sea is constrained by the shallow sill depth of 580 m. Recent moorred current observation reported that a mean transport volume via the Halmehera Sea is about 2.44 Sv with strong seasonal fluctuation of transport (Li et al., 2020). Ilahude and Gordon (1996) reported high-salinity values in the thermocline and lower thermocline of the SPSW downstream in the Seram Sea, and concluded that only thermocline and lower thermocline water were entering this portal; however, the very strong turbulent mixing of water masses in this sea (Koch-Larrouy et al., 2015; Koch-Larrouy et al., 2007) could modify this conclusion. Thus, the role and precise estimates of transport volume of South Pacific water into the ITF water

masses via this passage remain unclear (Atmadipoera et al., 2009; Gordon et al., 2010; Koch-Larrouy et al., 2007). More measurements are needed in the secondary inflow portals in order to better define the ITF origin.

In addition, from the INSTANT measurement (Sprintall et al., 2010, 2009), in northern Ombai Strait, an extension of the eastward South Java Coastal/Under Current (SJCC/SJUC) was found, depicted as two distinct cores of eastward flow at near-surface and intermediate depths, and associated with the presence of salty Indian water in the intermediate layer (Atmadipoera et al., 2009; Sprintall et al., 2009). One possible explanation is the penetration of highly variable North Indian Intermediate Water (NIIW) via the southern Lesser Sunda Islands into the Ombai Strait. NIIW, originated from the Red Sea overflow, is distributed along the equator in the Indian Ocean and is advected eastward and then south along the Indonesian archipelago (Wijffels et al., 2002). However, to date, no measurements on the pathway between Lombok and Ombai Straits have been taken to test this hypothesis. Therefore, the penetration of salty South Pacific water into the Halmahera Sea as well as salty intermediate Indian water into Savu Sea both remain unclear.

Vertical mixing due to internal tides has been identified to be extremely strong in the Indonesian seas. Hautala et al. (1996) used a simple advection-diffusion model with temperature and salinity profiles in the entrance and at the exits of the archipelago to demonstrate that a mean vertical diffusivity (K_z) of 1 to 2 10^{-4} m^2 s^{-1} was necessary to explain the water mass structure. However, more recent studies have shown that this mixing is strongly heterogeneous (Hatayama, 2004; Koch-Larrouy et al., 2015; Koch-Larrouy et al., 2007) with values as high as 10^{-2} to 10^{-1} m^2 s^{-1} above the sill. Koch-Larrouy et al. (2007), using a simplified parameterization, showed very large K_z values

in Halmahera and concluded that vertical mixing was the main cause of the SPSW erosion in this sea.

One of the main objectives of the Indonesian Mixing (INDOMIX 2010) experiment was to quantify the physical processes of the turbulent mixing of the ITF water using different independent methods of measurement (i.e., microstructure profiler, fine-scale methods and chemical passive tracer analysis) (Bouruet-Aubertot et al., 2018; Koch-Larrouy et al., 2015). In the Halmahera Sea, during the INDOMIX cruise, direct estimates of dissipation using the VMP (vertical microstructure profiler) show that K_z rises from $5x10^{-4}$ m^2 s^{-1} at the surface layer to 10^{-1} to 10^{0} m^2 s^{-1} at the bottom for stations C1 (950 m) and C3 (900 m) (Figure 1). In open basin areas, such as the Banda Sea, and in the center of the Halmahera Sea, Koch-Larrouy et al. (2015) found the vertical diffusivity much smaller (10^{-5} to 10^{-4} m^2 s^{-1}). These values are consistent with a recent study using Thorpe analysis of turbulent mixing, based on historical CTD datasets in Indonesian seas, which revealed much stronger turbulent kinetic dissipation rates on the order of 10^{-6} to 10^{-7} m^2 s^{-3} in several major ITF passages such as Labani, Dewakang, Halmahera, Lifamatola, and the main outflow straits (Purwandana et al., 2020). Results of a study using a high-resolution non-hydrostatic modeling approach also suggest that the bottom-intensified vertical structure of the dissipation rate is dominant in the ITF outflow straits region, while the effects in other areas are near-surface and thermocline intensified patterns (Wen et al., 2021). Modeling study in the secondary entry portal of the ITF in the Halmahera Sea demonstrated that the combined effect of tide-induced vertical and horizontal mixing can account for 90 % of the ITF water transformation (Nagai et al., 2017). More precisely, they conclude that the transformation of the ITF waters is dominated by tide-induced vertical mixing (76%), although there must be some additional mechanisms to

make up for the lack of water mass transformation such as horizontal mixing induced by the tides (14%). Very recent study on direct estimates of turbulent mixing in the Indonesian Seas has shown that some narrow tidal straits exhibit a strong turbulent mixing with large density overturns and high vertical diffusivity associated with downslope jets (Nagai et al., 2021).

In addition, this mixing has been shown to be relatively strong (10^{-4} m^2 s^{-1}) in the surface layer (Koch-Larrouy et al., 2015), where it may play a major role in bringing nutrient-rich deep water into the euphotic layer which would favor primary production. Although the potential impact of vertical mixing on primary production has been previously suggested to be important for both nutrients and resultant chlorophyll concentration (Koch-Larrouy et al., 2015; Sprintall et al., 2019, 2014), it has never been quantified or directly addressed in previous studies. The study related to biogeochemical properties measured during the INDOMIX cruise will be presented in a companion paper (Part 2).

In this paper, we use the INDOMIX dataset to describe the characteristics of the water masses in terms of all physical properties and dissolved oxygen concentrations. We describe the water mass properties along the eastern route, and provide new insights to better understand the transformation of salty SPSW from its entry portal in the Halmahera Sea, to the Seram Sea, the Banda Sea, and subsequently to its exit portal in Ombai Strait. We also investigate the distribution of Indian waters, sampled along the southern Lesser Sunda Islands from the Ombai to the Lombok Straits. We also investigate how the previous measured Kz (Koch-Larrouy et al. 2015) can explain the observed water mass transformation.

In this study, Section 2 describes the materials and methods, while Section 3 presents the results and discussion, including a snapshot of upper-layer circulation and

full-depth velocity profiles (Section 3.1), and description of the water mases properties, comprising the structure of ITF water, the stratification and distribution of ITF water masses (Section 3.2). Section 3.3 presents discussion, covering particular ITF characteristics in the study area, and proving that the very high vertical diffusivities estimated using the INDOMIX data (Koch-Larrouy et al., 2015) represent the main physical process to explain the water mass transformation. Finally, in Section 4 we summarize the results.

2. MATERIALS AND METHODS

2.1 The cruise track and stations

The INDOMIX cruise track started from the westernmost equatorial Pacific Ocean (PO) rims from the Halmahera Sea via the Seram Sea, Banda Sea, Ombai Strait, and along the southern coast of the small Sunda Arc, across the Lombok Strait, then to the Java Sea. The cruise took place onboard the R.V. Marion Dufresne from July 8 to July 19, 2010 (Fig. 1). Guided by previous work (Koch-Larrouy et al., 2007) that shows that high tidal energy appears in several key sub-basins, such as the Halmahera Sea (HS) and Ombai Strait (OS), we chose to focus on HS and OS areas as the main study locations of the INDOMIX cruise. For comparison, a secondary site with lower tidal energies was selected in the Banda Sea (BS). At the main sites, measurements of ~24-hour 'yoyo' conductivity-temperature-depth-dissolved oxygen (CTD-O) with SBE Seacat 911plus CTD were conducted. In addition, a pair of upward/downward-looking lowered acoustics Doppler current profilers (LADCP) RDI 300 kHz were used for full-depth velocity profiling, which was alternately conducted with VMP. Two CTD-O/LADCP-VMP profiles were collected at the secondary sites at the Pacific and Banda stations. Along the rest of the cruise tracks in the Seram Sea (CS), part of BS, and

along the southern Lesser Sunda Island (SA), a series of expendable CTD (XCTD) measurements were carried out with a sampling distance of about thirty nautical miles (0.5°). Table 1 presents a brief description of the CTD-O and XCTD station measurements. The INDOMIX cruise report was provided on the web and can be accessed publicly through the link: http://campagnes.flotteoceanographique.fr/campagnes/10200020/#.

2.2 The CTD-O and XCTD measurements

A SeaBird Electronics (SBE) 911plus CTD/Rosette was used for profiling of temperature, salinity, dissolved oxygen, and chlorophyll fluorescence values, in addition to a light transmissometer in the water column. The system was configured with an SBE-4 conductivity sensor with pump, an SBE-3plus temperature sensor, an SBE 43 dissolved oxygen sensor, a Chelsea fluorometer, a beam attenuation sensor, and 22 10-liter PVC rosette-bottle samplers out of a total capacity of 24 bottles; the remaining compartments were replaced with two 300 kHz upward/downward-looking lowered ADCP instruments.

Depending on the water depth at each measurement station, the instruments were lowered to close to the sea bottom, except for the XCTD measurements which have a maximum depth of about 1100 m. The deepest instrument measurement of CTD-O-Chl/LADCP was at the Banda station (~4435 m), followed by the Pacific station (~3020 m). In the Halmahera Sea, three sites were selected (Fig.1), located on the entrance sill slope (~950 m, site C1), in the central basin (~1450 m, site C2), and on the exit sill slope (~900 m, site C3). In the Ombai Strait, the measurement was performed on the northern entrance slope between Alor and Wetar Islands (~1500 m, site C5). A total of 42 CTD-O-Chl/LADCP and 21 XCTD casts have been acquired;

note that XCTD instruments are not equipped with dissolved oxygen (DO) and chlorophyll fluorometer sensors, thus at XCTD stations DO and Chl data are not available. A number of 176 seawater samples from various depth levels and stations were taken for CTD calibration purposes using 24 rosette bottles and two profiles for each CTD-O station. Bottle analysis for salinity and dissolved oxygen values was conducted onboard the Marion Dufresne.

Double bottle measurements of salinity were performed on board to examine the uncertainty of the measurement. Analysis of 28 samples taken from two Niskin bottles at the same depth level yielded mean measurement difference values of 0.001 psu and 0.2233 μmol/kg for salinity and dissolved oxygen respectively. Standard deviations of differences between samples are equal to 0.006 psu and 0.6252 μmol/kg for salinity and oxygen respectively. The root-mean-squared (RMS) value of differences between salinity sensor and bottle measurements is ±0.022 psu, with an uncertainty value for the salinometer of 0.001 psu.

The expendable conductivity-temperature-depth profiler (the XCTD) is a free-fall instrument for measuring the temperature and salinity profiles of the upper ocean. We used the XCTD-1 probe type, manufactured by Tsurumi Seiki Co. Ltd with a terminal depth of 1100 m; the depth equation used was the manufacturer's standard. The accuracy values of the temperature and conductivity sensors are ±0.02 °C and ±0.03 mS/cm, respectively, with a depth resolution of 0.0203 m. For the deck unit, we used an LM-3A handheld launcher manufactured by Lockheed Martin Sippican; the Sippican data acquisition software version was Win MK21.

A total of 21 XCTD profiles were collected during the cruise. One profile in the Sumba Strait was acquired down to only 500 m depth, thus we deployed the second full-depth profile. The raw XCTD data were converted by the Sippican MK21 software

and exported to text file format. A time-depth conversion was performed according to the manufacturer's equation for the XCTDs.

The methods described in Sloyan et al. (2010) and Uchida et al. (2011) were applied to process the XCTD data from the INDOMIX cruise; a brief explanation for processing of XCTD data is as follows. First, each profile was manually checked for outliers and these spurious data were removed. The first 4 m of the XCTD salinity profiles were then removed due to a delay in conductivity sensor readings (Tanguy et al., 2010). After applying a smoothing filter to the data with a 5-point weighted running-mean, the XCTD temperature-salinity profiles were compared to available CTD data from near the point of deployment. In the Banda Sea, a homogeneous layer in salinity is found at about 800 m depth (e.g., Ilahude and Gordon, 1996); here, the XCTD profiles were fitted to the CTD profiles at the reference 800 m depth. Identical data-processing was also applied to the XCTD data in the Seram Sea and along the southern Lesser Sunda Islands, where the depth of homogeneous salinity layers in CTD profiles were obtained at 900 m and 400 m depth respectively e.g., (Fieux et al., 1994; Molcard et al., 2001).

2.3 Underway shipboard ADCP and lowered ADCP measurements

The hull-mounted 150 kHz RD Instrument was used to measure underway SADCP current data with 5-minute averaging. The 150 kHz Ocean Surveyor was configured with 45 vertical bins with an 8 m bin size, a bin-blank length of 8 m, a transducer depth of 6 m, no bottom-track, and ping interval and heading offset equal to 0 s and 52.5° respectively. The CODAS3 program (Firing et al., 1995) was applied to process and correct SADCP data. Ancillary data included geographical positioning with GPS, surface temperature, sound speed, and gyrocompass.

The full-depth velocity profiling with LADCP was conducted simultaneously with lowering of CTD sensors to near bottom depths. For this purpose, two upward and downward-looking 300 kHz ADCP RDI broadband instruments were used and attached to the CTD frame. The bin length was set to 8 m and the time between pings was 300 ms. Processing of LADCP data was conducted using LDEO software version 8b (2004) described in Thurnherr (2011), which included the shear method (Firing et al., 1995; Fischer and Visbeck, 1993) and the velocity inversion method (Visbeck, 2002). In this study, results of the velocity inversion methods are presented and discussed for the 4 intensive CTD/LADCP "yoyo" stations (3 stations in Halmahera Sea and 1 station in Ombai Strait).

3. RESULTS

3.1 Upper-layer circulation and full-depth velocity profiles

Current velocity data sets from the SADCP at 150 kHz (ranging from 0 to 200 m depth), and 300 kHz upward/downward-looking LADCPs mounted on the rosette were analyzed to describe the snapshot of circulation during the cruise. The upper layer (i.e., the first 200 m depth) is well-documented by the SADCP, while the full-depth velocity profile is described by "yoyo" rosette profile at the 6 stations (from C0 to C5).

The upper 200 m depth current vectors along the cruise track (Fig. 2) exhibit strong flows (between 0.5 and 1 m s^{-1}) in regions of the ITF passage, namely the entry/exit portals of the Halmahera Sea, the Seram Sea, the Ombai Strait, and the Lombok Straits. Mean current vectors between 20–100 m depth provide information about upper-thermocline circulation (Fig. 2, upper panel), while the 100–200 m depth range provides the thermocline and lower-thermocline circulations (Fig. 2, lower panel).

In the Pacific section, west-southwestward flows are observed in both layers, with values of 0.4 m s^{-1} in the upper layer and 0.1 m s^{-1} in the lower layer (Fig. 2). When approaching the northern entry portal of Halmahera, the current vectors are mostly southward. In the central basin eastward currents may be associated with a localized small eddy structure, a feature also identified by simulations in the INDESO model (Nugroho et al., 2018) (not shown). At the exit portal of Halmahera, current vectors diverge between westward flow mainly in the upper layer and vigorous southward flow of about 1 m s^{-1} from the surface down to 200 m (Fig. 2, upper and lower panel, respectively). Across the Seram Sea, the flows are consistently southwestward, however, when approaching the Manipa Strait north-westward current vectors are evident and even stronger in the lower layer (Fig. 2, lower panel).

When entering the Banda Sea via the Manipa Strait, the flow becomes weaker with 0.2 to 0.3 m s^{-1} eastward flow from the surface to 200 m depth (Fig. 2). In the southern Banda Sea, the flow reverses westward with almost the same intensity as the surface layer, while between 100 and 200m depth the ITF eastward flow from Flores toward the Timor passage is visible south of 7 °S. This snapshot of current vectors along the north-south section in the Banda basin may indicate clockwise circulation in the upper 200 m depth. This cyclonic circulation is also found from recent modeling study of Zhu et al. (2019), suggesting that during the southeast monsoon period a clockwise circulation is established in the upper layer as a response to both the monsoonal winds forcing in central and eastern Banda, and the effect of Coriolis in the western and southern boundaries. The presence of clockwise upper layer circulation here can also be explained by a balance of potential vorticity flux and wind stress curl (Liang et al., 2019).

Strong south-westward flow appears in the Ombai Strait (Fig. 2 upper), which is well-documented as one of the ITF outflow portals (Sprintall et al., 2009). Here, ITF water from Flores and southern Banda is transported into the Savu Sea and then to the Indian Ocean. In the last section, along the Lesser Sunda Islands, current vectors seem to vary between eastward and northeastward flows. The alternate southward vs northward current vectors may indicate sub-mesoscale activity, constrained by the very narrow strait and semi-enclosed Savu Sea, which interact with westward coastal flow from the Ombai Strait. Strong southward ITF flow is evident in the Lombok Strait before entering the Bali Sea; in the surface layer (20–100 m depth) a southward flow is also coming from Sape Strait as described by Syamsudin et al. (2010).

In order to document the full-depth velocity profile, we used data from the repeated rosette-mounted LADCP acquired at stations C1, C2, and C3 in Halmahera and at station C5 in Ombai (Fig. 3 – Fig.6). In the entry portal of Halmahera (C1), the velocity profile exhibits a strong southward flow of up to 1m s^{-1} in the first 150 m and below 400 m depth (Fig. 3b); the first 150m shows consistently southward flow directions over the 24 h period, with a small decrease at 18:00. Below 400m, the flow reverses four times in 24 h, which is a signature of semidiurnal tides. In the intermediate layer, the flow is smaller with values below 0.6 m s^{-1}, showing opposing phase variations at semidiurnal frequency. This structure is the result of mode 3 semidiurnal internal tides superposed with a surface southward mean flow (Fig. 3c). The zonal flow exhibits a diurnal variation at 100 m depth and below 400 m (Fig. 3a). Baroclinic zonal and meridional current components (Fig. 3d and 3c) exhibit strong velocity (~0.8 m/s) in the upper 200 m but much weaker amplitude between 200 m and the bottom with diurnal and semidiurnal flow patterns for meridional component (Fig. 3e) are still visible.

At station C2 (central Halmahera basin), the current profile exhibits a south-westward flow (Fig. 4ab) with diurnal variation in the first 80 m and semidiurnal modulation at 150 m depth (Fig. 4b). At about 300 m depth, the meridional component indicates a relatively strong positive (northward) current (Fig. 4b). Baroclinic current components (Fig. 4de) are much weaker compared to that observed at the station C1 and present two cores of weak velocity (<0.2 m/s) in the upper 400 m depth for meridional component.

At the exit portal of Halmahera (station C3; Fig. 5ab), strong south-westward flow (>1.0 m/s) appears in the upper 100 m depth range. In addition, a clear signal of semidiurnal modulation is found at 200 m that reverses between 400 m and 800 m depth. This structure is typical of mode-3 internal tide, however, the structure is quite complex and may reflect higher mode structure (Fig. 5de).

At site C5 (Fig.6), strong semidiurnal tidal currents originating from the Indian Ocean (Hatayama, 2004; Robertson, 2010; Wyrtki, 1961) are found (Fig. 6b). Mean full-depth velocity profiles show a strong southward flow in the upper 700 m with two maxima, centered in the surface layer and at near 400 m depth. In the surface layer, maximum meridional velocity is approximately 0.6 m s^{-1} southward (Fig.6c); this persistent mean southward flow appears to represent Ombai ITF (e.g., Molcard et al., 2001; Sprintall et al., 2010, 2009). Time-depth sections of baroclinic velocity components indicate a fairly complex flow pattern, especially below 400 m depth (Fig. 6d-e lower panel). The negative baroclinic velocity component (i.e., southward) is dominant in the upper 400 m depth range.

3.2 Description of the water masses physical properties (T, S, O)

a) Water mass properties and transformation

In this section, we analyze temperature-salinity diagrams (Fig. 7a, T-S), temperature-dissolved oxygen diagrams (Fig. 7b, T-DO), and salinity-dissolved oxygen diagrams (Fig. 7c, S-DO).

Near-surface and thermocline water

The structure of water masses at station C0 (see Fig. 1 for station locations) consists of relatively warmer and saltier SPSW (Fig.7, black). Here the SPSW is characterized by a maximum salinity core layer of about 35.194 psu (Table 2), centered on a near surface density of 24.0 σ_θ (Fig. 7a), with a relatively homogeneous dissolved oxygen content of about 127 μmol/kg (Fig. 7b). Kashino et al. (1996) found much saltier SPSW of 35.375 psu at a CTD station located southeast of station C0, which could potentially be much closer to the source of SPSW drawn by the New Guinea Coastal Current and Under Current (Kashino et al., 2013, 1996; Kuroda, 2000).

At the entry portal of the Halmahera Sea located on the sill (station C1, Fig.7, dark red), constrained by a sill depth of ~650 m, a salinity maximum of the SPSW thermocline and lower thermocline water is predominant. At station C1, the salinity maximum of the SPSW slightly decreases to 35.051 psu, compared to a value of 35.194 psu at station C0. The potential density found at the bottom is about 27.0 σ_θ (Fig. 7a). A relatively homogeneous layer of dissolved oxygen (DO, between 120 and 140 μmol/kg) with linear variation between 5 and 25°C is found (Fig. 7b). The core layer of SPSW is indicated by maximum salinity (35.051 psu) and high DO (130 μmol/kg).

In the central Halmahera Sea basin (station C2, red, Fig. 7), the structure of the salinity maximum of the SPSW is characterized by two patterns: 1) where isopycnal

density values are below 24.0 σ_θ and above 26.5 σ_θ, the T-S profiles are similar to those observed at the exit portal of Halmahera (station C3, light red); and 2) between the isopycnal surfaces of 24.0 σ_θ and 26.5 σ_θ, the T-S profiles largely overlie those measured at the inflow portal (station C1, dark red), but there are also prominent inter-leaving (zigzagging) features in salinity (Fig. 7a). These features are also consistently shown in the T-DO diagram (Fig. 7b). For example, at densities greater than 26.5 σ_θ, the oxygen content is almost identical to those observed at station C3. However, no interleaving features in oxygen content are found, perhaps due to quasi-homogeneous oxygen centration at these layers.

Within the segment of interleaving salinity values at station C2, particularly between the isopycnal of 24.5 σ_θ and 25.0 σ_θ (the center of SPSW core layer), the observed salinity is larger than that measured at station C1 and closer to the value measured at station C0 (Fig. 7a). This suggests that there could be another inflow portal for SPSW in this layer. From the bathymetry measured during the cruise (not shown), a deeper passage was identified north of station C1 with a sill depth of 950 m.

A near-total extinction of the salinity maximum SPSW core occurs in the Seram Sea (yellow line in Fig. 7a), where its high-salinity is almost entirely replaced by less salty, homogeneous in salinity water between surface densities of 22.0 σ_θ and 25.0 σ_θ (note that in the Seram XCTD section, there was no dissolved oxygen measurement). Here, the salinity maximum of the SPSW is around 0.5 psu lower than that observed in the Halmahera Sea (35.02 psu). In addition, at the last two stations in the Manipa Strait (light green, Fig. 7), the salinity maximum is at 34.5 psu from the 5 °C to 25°C isotherms.

The structure of water masses in the Banda sea is indicated by near-surface fresh water above surface density 23.5 σ_θ, originating from the western ITF region, and a

relatively homogenous water in salinity between the thermocline and intermediate layer (i.e., between surface density 23.5 σ_θ and 26.5 σ_θ) (Fig. 7a), in good agreement with findings from previous studies (Atmadipoera et al., 2009; Ffield and Gordon, 1992; Gordon, 2005; Ilahude and Gordon, 1996; Wyrtki, 1961). Wyrtki (1961) named these thermocline and intermediate water masses as the Banda Thermocline Water and Banda Intermediate Water respectively. Within the near-surface layer (above surface density of 22.5 σ_θ) two water masses are identified: one comprising saltier water, occupying the area between northern and central Banda, and the other as fresher water occupying the southern area (Fig. 7). By considering the T-DO and S-DO diagrams, the structure of the water mass in central Banda shows that near-surface and thermocline Banda water is represented by much higher temperature values with a rapid decrease in oxygen content. This pattern is distinctive, compared to Ombai water (green curve in Fig.7) which has homogeneous values in near-surface salinity and temperature (Fig. 7b and 7c).

In the Ombai Strait, CTD-DO profiles were collected in the northern entrance slope of ~1500 m water depth between Alor and Wetar Islands. To capture the different source of water masses from Flores and Banda, 5 casts were conducted closer to the western side and 4 casts to the eastern side (separating by a distance of ~25 km). Near-surface and thermocline fresh water are clearly seen (blue and light blue curves in Fig. 7a), which are suggested to be derived from Throughflow Makassar water mixed with fresh surface Java Sea water. This is in good agreement with past studies (e.g., Atmadipoera et al., 2009). Fresher thermocline water is centered on near surface density 24.0 σ_θ with much fresher values observed in the western site (blue curve) than those observed in the eastern area (light blue curve in Fig. 7). In contrast to the Banda water, much colder water is found in Ombai (Fig. 7b). Although the northern entrance

of Ombai is fairly narrow (about 25 km width) between Alor and Wetar, the structure of the water mass, as sampled at the western and eastern side, is somewhat different (blue and light blue curves in Fig. 7a). This suggests that relatively warmer and saltier Banda thermocline water (light blue curve) follows the eastern side within the northern entrance of Ombai, while the remainder (blue curve) passes partly via the western side directly from the Flores Sea.

Within the southern Lesser Sunda Islands section, very fresh near-surface and thermocline water is found (violet – dark violet curves in Fig. 7a). Spatial zonal variations in salinity in the thermocline layer are present in the east-west section, where relatively much fresher water appears in the eastern area, in contrast to saltier water in the western area (dark violet).

Intermediate and deep water

At station C0, on the Pacific side (black curve in Fig. 7), there are several water masses occupying the intermediate layer between surface densities of 25.5 σ_θ and 27.5 σ_θ (Table 2), which consist of salinity minimum (34.640 psu) and high oxygen content (>133 μmol/kg) water with near surface density of 25.9 σ_θ; salinity minimum (34.762 psu) and oxygen minimum (131 μmol/kg) water with near surface density of 26.4 σ_θ; salty (34.859 psu) and high oxygen (135 μmol/kg) South Pacific Subtropical Lower Thermocline Water (SPSLTW) centered near a surface density value of 26.53 σ_θ; salinity minimum (34.537 psu), potential temperature 6.8 °C, and relatively high oxygen (>110 μmol/kg) Antarctic Intermediate Water (AAIW) centered on a near surface density value of 27.2 σ_θ; water with a salinity minimum (34.550 psu), potential temperature of 4.7 °C, an oxygen minimum (<100 μmol/kg), and near surface density of 27.3 σ_θ, representing equatorial Pacific water (eqPW) (Kashino et al., 1996); and the

deep water-mass of the Antarctic Bottom Water (AAIB) is characterized by high oxygen (>110 μmol/kg), a potential temperature of 5 °C, and relatively salty water (>34.6 psu), with surface density > 27.6 σ_θ. The characteristics of these water masses around site C0 confirm the findings of previous studies (e.g., Atmadipoera et al., 2009; Kashino et al., 2013, 1996).

A double salinity minimum occurs at near surface density values of 26.5 σ_θ (with high oxygen), and 27.2 σ_θ (with low oxygen), suggesting the presence of various overlapping intermediate water masses around the region (e.g., NPIW and AAIW water origin); this finding is in good agreement with previous studies e.g., (Kashino et al., 1996; Wyrtki, 1961).

In the Halmahera section, the water mass in the intermediate layer is occupied by the lower part of SPSW, known as the South Pacific Subtropical Lower Thermocline Water (SPSLTW), centered on a surface density value of 26.5 σ_θ. In the inflow portal of C1, the salinity of this water mass is 34.75 psu and oxygen >120 μmol/kg. However, in the two consecutive stations (C2 in the central basin, and C3 in the exit portal), salinity and oxygen are already reduced by about 0.2 psu and to <110 μmol/kg respectively. Constrained by the topographic sill depth (< 700 m) surrounding the Halmahera basin, the potential density at the maximum depth for the three stations is only about 27.0 σ_θ. This means that no deep-water masses are found in the deeper part of Halmahera basin. However, the upper part of intermediate water (AAIW), centered on an isopycnal value of 27.2 σ_θ, may be advected into the Halmahera basin, since the temperature-salinity-oxygen structure of the Halmahera basin is aligned with the water mass of the Pacific side at station C0 (Table 2).

In the Seram section, the salinity of SPSLTW, with a near surface density value of 26.5 σ_θ, is markedly reduced to about 34.66 psu, with only small variations spatially

(less than 0.1 psu); this water mass is therefore fairly homogeneous in salinity (Fig. 7a). However, near the center and lower thermocline depths, for example, at surface densities of 23.5 σ_θ and 25.0 σ_θ, the intermittent appearance of salinity maximum SPSW is clearly observed. The possible mechanism to this SPSW transformation is associated with an intensive vertical mixing due to breaking of internal tides and also horizontal mixing due to the sub-mesoscale eddies activities (Nagai et el., 2017).

In the northern part of the Banda section, the signature of relatively salty SPSLTW (~34.636 psu) with near surface density of 26.5 σ_θ is clearly seen (Fig. 7a), and its high-salinity core decreases toward the south. At the central Banda Sea station (station C4), relatively homogeneous intermediate water mass is observed; this is characterized by a salinity of 34.556 psu, oxygen content of ~100 μmol/kg, and a temperature of 10.6 °C, centered on a near surface density value of 26.5 σ_θ (green curves in Fig. 7a-c) (Table 2). This distinct water mass has been referred to in previous studies as the Banda Intermediate Water e.g., (Broecker et al., 1986; Ilahude and Gordon, 1996; Wyrtki, 1961) or Indonesian Intermediate Water (IIW), which is interpreted as a fresher, homogeneous, intermediate water mass moving downward in the Indian Ocean (Fieux et al., 1994; Talley and Sprintall, 2005; Wijffels et al., 2002). During this cruise, the signature of the SPSLTW in central Banda (station C4) was not captured. However, during the other monsoon period, for example in February, previous studies (e.g., Atmadipoera et al., 2009; Ilahude and Gordon, 1996) note that the presence of SPSLTW was remarkably clear in the southern Banda Sea, closer to Ombai. In the southern part of the Banda section, the intermediate SPSLTW water is completely replaced by minimum salinity North Pacific Intermediate Water (NPIW) drawn by the ITF from Makassar.

When the T-S-DO diagram is examined in more detail, another intermediate water mass is identified, centered on a near surface density value of 26.8 σ_θ, characterized by distinctly low oxygen (< 90 μmol/kg), relatively high salinity (34.585 psu), and cool temperature (8.3 °C) near 500 m depth (Table 2). Gordon et al. (2003) suggested that the Banda Intermediate water is supplied by both North Pacific Intermediate Water (NPIW) via Makassar and Antarctic Intermediate Water (AAIW) through the Maluku Sea, as indicated by salinity and oxygen minima. Wyrtki (1961) also proposed that the Banda Intermediate Water is influenced by salty, low oxygen North Indian Intermediate Water (NIIW) entering through Savu and Ombai. With only two CTD-DO profiles in the central Banda Sea, it is unclear whether the relatively saline and low oxygen intermediate water observed during the cruise at Banda site C4 is part of NIIW or AAIW. However, the intermediate water mass in Ombai also shows an oxygen minimum (see C5 next paragraph).

Banda Deep Water (below surface density of 27.5 σ_θ to the bottom) is indicated by a slight increase in salinity (34.617 psu) and dissolved oxygen (>100 μmol/kg), with a potential temperature of 2.8 °C below 3000 m depth (Fig. 7, green; Table 2). An increase in oxygen is suggested to relate to the supply of relatively high oxygen water masses via the deep overflow Lifamatola passage (Broecker et al., 1986; Gordon et al., 2003; Van Aken et al., 1988; Wyrtki, 1961).

In the western edge of Ombai (station C5, light blue-blue in Fig.7), intermediate water with a near surface density value of 26.5 σ_θ is indicated by a salinity minimum (34.494 psu) but moderately high oxygen content (>100 μmol/kg) (Fig.7), which represents North Pacific Intermediate Water drawn by the ITF from Makassar to Flores and then to Ombai, as confirmed by previous studies (Atmadipoera et al., 2009; Gordon et al., 2003; Ilahude and Gordon, 1996). In the eastern edge of Ombai, the salinity

value is slightly higher (34.543 psu) and oxygen concentration >100 μmol/kg. Its characteristics are consistent with Banda water at station C4; here, an oxygen minimum is recorded (<90 μmol/kg), with a salinity of 34.562 psu and a near surface density of 27.2 σ_θ (near 1540 m depth) (Table 2). Compared to Banda station, the salinity is slightly lower but the oxygen content is higher, hence, it is likely that the water mass with an oxygen minimum and slightly high salinity near a density value of 27.2 σ_θ could be North Indian Intermediate Water (NIIW) in origin. The structure of water masses in Ombai and Banda with near surface densities of 27.5σ_θ is identical, where the salinity and oxygen values are relatively high compared to water with near surface density of 26.6 σ_θ (Fig. 7).

From XCTD data along the northern Savu section, the structure of salinity maximum NIIW is clearly shown between potential density anomalies 26.8 σ_θ and 27.2 σ_θ (centered on surface potential density anomaly 27.0σ_θ) (Fig. 7a, violet). Salinity maximum NIIW of 34.702 psu with a temperature of 8.28 °C predominates in the westernmost stations, with the salinity maximum decreasing toward the east.

b) Vertical structure of temperature profiles

Our data clearly indicate that the thickness of the warm surface layer and the thermocline layer increase from the Pacific Ocean to the Indian Ocean (Fig. 8). Warmer surface water with an isotherm value above 29 °C appears in the first four measurement stations in the Pacific Ocean, Halmahera Sea, and some of the Seram stations. This represents equatorial warm water advected from the western Pacific warm pool water that flows into the Halmahera Sea (see the following section on water mass analysis). The homogeneous temperature layer (>29 °C) in the Pacific Ocean (station C0) is relatively deep, at about 90 m. Station C0 is located in the open ocean and confined

within the western boundary current, with influence from both the Guinea Coastal Current and Under Current (e.g., Kashino et al., 2015). The deep homogeneous layer in temperature is therefore enhanced by the western boundary current system rather than generated directly by surface winds (Ando and Hasegawa, 2009; Kara et al., 2003; Kashino et al., 2013; Kuroda, 2000; Lukas and Lindstrom, 1991). Within the Halmahera Sea, the surface homogeneous warm layer varies in maximum depth from 50 m in the entry portal (C1) to about 25 m in the exit portal (C3). In the Banda Sea and Ombai Strait, this warm layer can be found down to about 75 m depth (above the 27 °C isotherm), enhanced directly by strong persistent southerly monsoon winds.

Indeed, during the cruise, strong surface winds of over 24 m s^{-1} were recorded over the Banda Sea and Ombai Strait. Following Geary (2012), an empirical calculation of the wind-induced mixed layer depth, using a wind speed of 12 m s^{-1}, yields a value of about 44.1 m. Here, with the observed speed of 24 m s^{-1} in the Banda Sea, the mixed layer depth is found to be about 75 m, which is consistent with the Geary (2012) calculation. Along the southern coasts of the Lesser Sunda Islands, the surface temperature varies between 25 °C and 27 °C; colder temperatures are recorded near the Sumba Strait, which may be associated with Ekman upwelling events that occur during the southeast monsoon period (Potemra, 2003; Sprintall et al., 2010, 2003).

Below the surface layer, large vertical fluctuations in the thermocline layer are revealed between the 12 °C and 29 °C isotherms; at station C1, these fluctuations were as strong as 40–50 m for the 26°C isotherm. Similarly, at C2 and C3 we observe fluctuation of the isotherms, but with smaller vertical displacements (20–30m maximum). This large vertical fluctuation of isotherms is the results of strong internal tidal activity in the region, as also noted in previous studies (Koch-Larrouy et al., 2015; Nugroho et al., 2018), where isopycnal displacements were found in the INDOMIX

data and the INDESO model to be as large as 40 m. The center of the thermocline depth, as represented by the 20 °C isotherm, fluctuates between ~190 m on the Pacific side to ~150 m in the Halmahera Sea, and shallows to ~100 m in the Banda Sea and Indian Ocean side (Fig. 8). Below the lower thermocline layer, large undulations of the isotherm 9 °C are also consistently observed. The amplitude of 9 °C isotherm fluctuation is about 100 m in the Halmahera Sea (stations C1 and C2) and ~50 m at the Ombai stations (Fig. 8).

The 8 °C isotherm in the Pacific Ocean and in the Seram and Banda Seas is recorded at almost at the same depth level (550 m depth). However, in the Halmahera Sea, this isotherm deepens to about 1100 m, indicating that relatively warmer water exists at a greater depth. Furthermore, near the 1000 m depth level, a temperature difference of about 3 °C is found between the Halmahera Sea and Banda-Ombai, where much warmer water of about 8 °C is situated in Halmahera Sea.

Below 500 m depth, a contrast in the temperature stratification or gradient between Halmahera and other areas along the cruise track is evident. The potential temperature in the Halmahera basin is warmer than that observed in the Pacific Ocean or on the Seram to Indian Ocean side. The 8 °C isotherm deepens to about 1100 m depth in the Halmahera basin (Fig. 8), but in other areas, the isotherm of 8 °C is found at depths between 450–550 m. Much colder water is observed in the Pacific and Banda-Ombai sides, with isotherm values of 3 °C and 3.5°C respectively at about 1400 m depth.

c) Vertical structure of salinity profiles

Cross-sections of salinity (Fig. 9) demonstrate a contrasting feature in salinity fields with saltier Pacific and Halmahera water (isohaline between 34.3–34.5 psu) and

fresher Banda to Savu waters (isohaline between 33.4–34.0 psu) in the upper 100 m depth range. Furthermore, in the thermocline, high salinity values are observed in the Pacific and Halmahera Sea, showing the presence of SPSW, with a salinity maximum between 34.65 and 35.1 psu, as described in the previous section.

The extension of the isohaline 34.9 psu tongue in Halmahera shows considerable fluctuation, and this isohaline feature is no longer observed at the exit of Halmahera (station C3). In contrast to the Pacific station (C0), the vertical extension of salty water (isohaline >34.65 psu) is down to only 400 m depth, however, in Halmahera Sea this isohaline is much deeper and a relatively homogeneous layer in salinity is recorded there.

In contrast, in the Banda Sea and Ombai Strait, the Java fresh tongue signature is observed with salinity values below 33.9 psu in the first 100 m depth range and potential density anomaly below 22.5 kg m^{-3}. Below, the Indonesian Throughflow Water (ITW) is found in the thermocline and intermediate layers (100 m and 800 m) with a homogeneous salinity near 34.6 psu.

The salinity distribution below 500 m depth is characterized by less saline homogeneous water in the Pacific and Banda-Ombai sides, however, in the Halmahera Sea, the salinity is slightly higher. A salinity core layer (>34.65 psu) is evident in the Savu Sea (Fig. 9). Below 500 m depth, much colder waters on the Pacific and Halmahera to Ombai sides contribute much denser water with isopycnal values above 27.0 kg m^{-3} (Fig. 10). In the Halmahera Sea, however, the warmer creates lower densities. Between 500 m and 1500 m depth, the oxygen content is characterized by two regimes: less oxygen content (<100 µmol kg^{-1}) on the Pacific and Banda-Ombai sides, and higher and homogeneous oxygen near 120 µmol kg^{-1} in the Halmahera Sea

where intense diapycnal mixing occurs (Bouruet-Aubertot et al., 2018; Koch-Larrouy et al., 2015).

d) Vertical structure of density profiles

The observed density sections are mainly dominated by the thermic effect which show similar patterns to the temperature profiles. Large fluctuations of the pycnocline are observed (Fig. 10), similar to those in the thermocline (Fig. 8) (for example, the isopycnal value of 24.5), in the entry portal of the Halmahera Sea and the Ombai Strait. These reflect strong internal tide activity, in good agreement with observations by (Koch-Larrouy et al., 2015), but in this study, the variability of the isopycnal depth is even greater.

Fluctuation of mixed layer depth (MLD) along the cruise track (Fig.10) revealed much deeper MLD at the first two stations (C0 and C1), in Banda (C4) and Ombai (C5). In contrast, very shallow MLD is found in central Halmahera (C2), in part of C3, and along the southern Sunda Arc. At C0, deeper MLD may be associated with the existence of a strong boundary current of NGCC (Fig. 2), but in Banda, a deepening MLD is induced directly by strong southeasterly winds (not shown). Deeper MLD at Halmahera (C1 & C3) and Ombai (C5) is caused by strong internal tidal waves (Bouruet-Aubertot et al., 2018; Koch-Larrouy et al., 2015) which were observed during the cruise. In the Halmahera basin, the 27.0 kg m^{-3} isopycnal drops to about 1300 m depth, compared to 500 m depth for the Pacific and Seram to Banda stations; this is principally due to the shallow 500 m depth of the northern strait of the Halmahera Sea.

At the end of the INDOMIX cruise track, off Lesser Sunda Islands, isopycnal 22.0 kg m^{-3} reaches the surface due to the presence of much colder and saltier local water masses that were created by coastal Ekman upwelling (Sprintall et al., 2010).

Higher densities are contributed by higher salinity and lower temperatures in the upwelling area which are found consistently in the along-track measurements of both surface temperature and salinity at 5 m depth (not shown).

e) Vertical structure of dissolved oxygen profiles

A high dissolved oxygen content (>180 µmol kg^{-1}) is found at all stations along the cruise track in the upper 50 m depth within the mixed layer (Fig. 11) in equilibrium with the atmosphere. Indeed, the Apparent Oxygen Utilization (AOU) at the sea surface with a salinity value of 34.4 psu, temperature of 29 °C, and dissolved oxygen content of 180 µmol kg^{-1} (typical surface values for stations C0 up to C3, so for the Pacific Ocean to the Halmahera Sea) yields an AOU value of about -14 µmol kg^{-1}. An AOU value of -17 µmol kg^{-1} is obtained using a salinity value of 33.9 psu, temperature of 25 °C, and dissolved oxygen of 190 µmol kg^{-1} (typical surface value for stations C4 to C5 in the Banda Sea and Ombai Strait). Thus, the surface waters in the mixed layer are closed to saturation compared to the atmosphere for oxygen concentrations. We can therefore conclude the mixed layer is in equilibrium with the atmosphere. A sharp vertical gradient of oxygen with some undulations is found in thermocline layer, with O_2 concentrations between 140 and 180 µmol kg^{-1} (Fig.11). In the Pacific Ocean, a homogeneous layer in oxygen (above the contour of 130 µmol kg^{-1}) occurs between 150 m and 350 m depth, and a relatively lower oxygen content (<120 µmol kg^{-1}) below 400 m depth, typical of the Pacific Ocean with a longtime residence for the deep waters. However, in Halmahera, a much higher oxygen content (about 120 µmol kg^{-1}) is observed down to depths of about 1000 m. In the Seram Sea, no oxygen data is available (Fig. 11) because only XCTD measurements were collected. Low dissolved oxygen content (<120 µmol kg^{-1}) is revealed in the Banda and Ombai areas below 300

m depth, with the oxygen minimum layer found beneath 400 m depth showing oxygen content values of <100 μmol kg^{-1}, which are close to the range for hypoxia ($[O_2]$ <60–80 μmol kg^{-1}) (Fig. 11) due to a strong surface stratification (Fig. 10) and an intense remineralisation of export production from the productive surface layer (higher chlorophyll concentrations) (see the discussion below). More details on this subject will be given in part II of this study.

3.3 Discussions

a) Depth of the northern portal in the Halmahera Sea

Water mass analysis from the INDOMIX cruise provides new insights which suggest that the northern portal of the Halmahera Sea could be deeper than previously documented. Within the region of inter-leaving salinity at station C2, particularly between isopycnal values of 24.5 σ_θ and 25.0 σ_θ (the center of the SPSW core layer), the observed salinity is greater than the value measured at station C1 and closer to the one measured at station C0 (Fig. 7a). This suggests that there could be another inflow portal for SPSW in this layer. From the bathymetry measurements recorded during the cruise (not shown), a deeper passage north of station C1 was identified, with a sill depth of 950 m.

Bathymetry profiles across the entry portal of the Halmahera Sea have not previously been measured. Luick and Cresswell (2001) found a sill of about 550 m depth before the entry portal of Halmahera passage, on the Pacific Ocean side. To address this issue, during the INDOMIX cruise, multi-beam echo-sounder (MBES) measurements were carried out at the entry portal of Halmahera, along a cross-section between the small island of Gebe and near the Patani peninsula of Halmahera Island (Fig.1). In this cross-section, we found the deepest channel of about 950 m was located

north of C1, and bathymetry is much shallower to the east closer to Gebe Island (Fig.1). The sill depth at the northern entry portal is a major constraint on the flow from the Pacific into the Halmahera Sea.

There are two possible inflow channels from the Pacific to the Halmahera Sea: firstly, west of Gebe channel (i.e., along the route between stations C0, C1 and C2), or, secondly, east of the Gebe channel, however, no measurements were recorded in this area during INDOMIX. Thus, the renewal of Pacific water masses into Halmahera may be derived from these two channels. In addition, the existence of simulated twin-eddies from INDESO model (Tranchant et al., 2015) within the Halmahera basin (not shown) may contribute to the inter-leaving processes where older water masses are mixed together with newer water entering directly from the inflow channels.

b) Inter-leaving features in salinity

On a much larger spatial scale, inter-leaving features in salinity in the western equatorial Pacific Ocean, referred to as the double salinity maximum, have been considered to be formed simply by renewal of salty water masses that are advected by the western boundary current system into the older water mass (Wyrtki, 1961). Furthermore, Kashino et al. (1996) also found similar features in the western equatorial Pacific, where the salinity minimum of NPIW converges with the lower part of the salinity maximum of SPSW at the same depth level.

To our knowledge, however, the inter-leaving of salinity features in the Halmahera Sea basin has not been previously documented. We hypothesize that strong mixing at the entrance sill and exit sill portals can modify density, such as via density currents, that may result in the formation of strong inter-leaving features. With this mechanism, it is likely that ‘new’ salinity maximum SPSW is advected from the entry

portal (C1) into the 'older' existing water mass in the central basin (C2). At the exit passage (C3), the salinity maximum value of SPSW reduces to about 34.905 psu. Below a density of 24.0 σ_θ, the extinction of salinity maximum of SPSW is clearly seen (Fig. 7a).

Inter-leaving of water masses may potentially be associated with intense lateral mixing induced by internal tidal waves. Koch-Larrouy et al. (2015) found a strong vertical diffusivity coefficient (Kz) at stations C1 (entry portal) and C3 (exit portal), but a weak Kz value at C2 (central Halmahera basin) (Fig. 3, in Koch-Larrouy et al., 2015). This suggests that the products of mixed salinity maximum SPSW water within the thermocline and lower thermocline layers (between isopycnal values of 24.0 and 26.0 σ_θ) at C1 may be drawn laterally by the flood-tide into C2 in the central Halmahera basin. On the other hand, during ebb tide water masses from C3 appear to be drawn into the central Halmahera Sea. Thus, the inter-leaving of salinity appears more intense in the thermocline and lower thermocline layers in the central Halmahera basin.

c) Drastic erosion of SPSW signatures in Seram Sea

The INDOMIX study, for the first time, provides continuous CTD data between the Halmahera and Seram seas and shows that the maximum of salinity is eroded within Halmahera Sea, with almost no more signature of this feature present in Seram Sea.

In the Seram section, upper-layer circulation (50–100 m depth) indicates a partitioning of strong westward flow from the exit portal of the Halmahera Sea into the Maluku and western Seram seas and southward into eastern Seram. A relatively weaker northward flow from the Manipa Strait is evidenced (Fig. 6a). This implies that upper salty water above a surface density value of 23.0 σ_θ is not found in the northern Banda section (Fig. 4), but may be rerouted into the Maluku and eastern Banda seas. In

contrast, in the thermocline layer (100–300 m) the northward flow from the Manipa Strait is stronger and westward flow into Maluku is weaker. As a consequence, the convergence of salty water from Halmahera and fresher water from the Manipa Strait results in a drastic transformation of SPSW with a salinity difference of 0.4 psu. Furthermore, the Seram Sea exhibits strong vertical mixing in the adjacent straits; the exit portal of the Halmahera Sea and Manipa Strait, sampled during the INDOMIX cruise, and both Lifamatola and the western Seram passages are also interpreted as exhibiting strong mixing (Koch-Larrouy et al., 2015). The mixing in these four passages could strongly alter the two convergent water masses and explain the pronounced transformation of the water mass.

A drastic extinction of the salinity maximum of the SPSW core occurs in the Seram Sea, where the salinity maximum is almost entirely replaced by fresher homohaline water in the thermocline. Two possible mechanisms are likely to occur. Firstly, partitioning of the flow may occur from the Halmahera Sea into Maluku Sea, Seram Sea and Outer Banda Arc (as shown in section 3.1, from SADCP data). By this mechanism, the flow into the Maluku and Seram Seas may already be significantly reduced. In addition, in the thermocline layer, northward flow was observed in the Manipa Strait (see section 3.1) that transports less salty water from Banda into the Seram Sea, which may also renew the Seram Sea with fresher water. Secondly, intense vertical mixing between salinity maximum SPSW and fresher surface and intermediate layers was documented in Koch-Larrouy et al. (2015, 2007), which has been shown to be capable of such rapid water mass transformation.

In the following section (*Section 3.3-e*) we propose a simple diffusion model which shows the mixing measured by INDOMIX is capable, after 2 days' residence time, of fully reproducing the observed vertical profile of physical properties (Fig. 12).

In addition, recent high-resolution modeling by Buijsman et al. (2016) (not shown) (from which Fig. 9 is extracted) showed very strong dissipation at C1 and C3, and even higher dissipation values in the northern part of Buru Island, in Lifamatola, and in the Manipa Strait.

During the INDOMIX experiment, there were no microstructure measurements in the Seram Sea. However, indirect fine-scale analysis using Thorpe's methods (Dillon, 1982) on the INDOMIX XCTD data from the Seram Sea shows that at the northeastern entrance of Seram, as well as in the Manipa Strait, vertical diffusivity (Kz) is relatively strong (Koch-Larrouy et al., 2015), in good agreement with model predictions (Koch-Larrouy et al., 2007). Previous studies, using fine-scale analysis applied to XBT data, showed significant fine-structure between Lifamatola (northern entrance of Seram Sea) and the Manipa Strait (Ffield and Robertson, 2005), in good agreement with INDOMIX data. High dissipation rate estimates from archive CTD datasets are also found in Lifamatola (Purwandana et al., 2020).

d) Strong vertical mixing as the main factor for physical tracer properties in the Halmahera Sea

In this subsection, we apply the mixing parameters measured in the Halmahera Sea from direct VMP microstructure calculated in Koch-Larrouy et al. (2015) to the physical tracers (temperature, salinity) at the entrance of the Halmahera Sea at site C0. We show that with reasonable assumptions of the residence time, that we justify below, we can explain the drastic change between Pacific water and Halmahera Sea water in terms of heat and salt using the vertical diffusivity as measured during INDOMIX, meaning that vertical mixing is at first order responsible for such erosion as described in the previous subsection.

The Kz value is estimated using VMP data, as described in Koch-Larrouy et al. (2015). It is shown that vertical diffusivity in the thermocline is remarkable at the entry and exit portals of Halmahera (sites C1 and C3) with values ranging between 10^{-3}–10^{-1} m^2 s^{-1} (Fig. 12). However, relatively weaker mixing is estimated in the central basin of Halmahera (site C2), with a value of 10^{-4} m^2 s^{-1}.

The unknown variable in this problem is the duration of exposition to this mixing; this is dependent on the timescale of mixing events and the residence time over the mixing region. Evaluation of this variable with precision is challenging, and no observations are available to constrain it. In this study, we produce estimates of residence time based on the advection measurements of INDOMIX (*section 3.3.e*) and using the INDESO model (Nugroho et al., 2018; Tranchant et al., 2015).

We define 3 layers of different advection regimes, based on the ADCP data (*Section 3.1*). Based on Fig. 8, at station C1 these regimes are: 1) Surface layer (0-100 m); 2) thermocline layer (100-300 m); and 3) deeper layer (300-950 m). The velocity across the strait has an average intensity of 1 m s^{-1} in the surface layer, 0.5 m s^{-1} in the thermocline layer, and 0.1 m s^{-1} elsewhere.

As for the spatial extent of the mixing region, we used the results of two different models, described in Nugroho et al. (2018). The generation of internal tides is calculated using the Ocean General Circulation Model NEMO (Bourdallé-Badie et al., 2019; Madec, 2014) using the conversion rate from barotropic to baroclinic tidal energy (Nugroho et al., 2018). We found that a mean value of 20 km around the sill showed the highest dissipation rate, mixing regime, and mixing events; we also assumed that the water mass is exposed to Kz as measured at C1 for a distance of 20 km, with the previously described velocity values for each layer, corresponding to a residence time

of 0.25 days for the surface layer, 0.5 days for the thermocline layer and 2 days for the deeper layer.

The results of this analysis are shown in Fig. 12. Using the same assumptions for the southern sill, we apply the Kz estimated over C2 and C3 for each layer for the same duration as for site C1. At C2, values of Kz are too small and the vertical profile of tracers does not evolve. For site C3, results are shown in the last two columns of Fig. 12. After 2 days residence time exposed by Kz1 and 1 day by Kz3, diapycnal mixing explains almost all the water mass transformation (Fig. 12). Indeed, temperature and salinity profiles calculated by the 1D mixing hypotheses (red line) show very good agreement with the observed mean profiles over the sea (black thick line). After 4 days (not shown), the results remain almost unchanged, suggesting a minimum energy threshold is required to thoroughly mix the water mass.

This calculation allows us to conclude that vertical mixing induced by the tides is the main source of water mass transformation. This result is in good agreement with the estimates Nagai et al. (2017) suggesting that 76 % of the ITF water mass transformation in the Halmahera Sea is done by the vertical tide-induced mixing.

e) Homohaline structure in Banda

The structure of water masses in the Banda Sea section is indicated by near-surface fresh water above a surface density value of 23.5 σ_θ, originating from the western ITF region, and a relatively homogenous water in terms of salinity between the thermocline and intermediate layer (between surface density values of 23.5 σ_θ and 26.5 σ_θ) (Fig. 7), in good agreement with previous studies (Atmadipoera et al., 2009; Ffield and Gordon, 1992; Gordon, 2005; Ilahude and Gordon, 1996; Wyrtki, 1961). Wyrtki (1961) named these thermocline and intermediate water masses as the Banda

Thermocline Water and Banda Intermediate Water. This water mass, characterized by its homohaline structure at 34.6 psu, is well documented (Atmadipoera et al., 2009; Gordon et al., 2003; Hautala et al., 1996; Koch-Larrouy et al., 2007), and is the result of strong mixing between the salty SPSW and the fresher NPIW entering via Makassar and very fresh surface water of the Java sea (Atmadipoera et al., 2009; Koch-Larrouy et al., 2008).

The occurrence of homogeneous intermediate waters in Banda are widely documented to be related to an oxygen minimum associated with biological processes that consume dissolved oxygen (Broecker et al., 1986; Van Aken et al., 1988; Wyrtki, 1961). This oxygen minimum is also found in Ombai below surface density values of 26 σ_θ. Since the Ombai area is influenced by ITF water, it is likely that the oxygen minimum water masses within the Ombai area are derived from Banda. It is also possible that in the deeper layer, water with an oxygen minimum is drawn from the Savu Sea into Banda/Flores Sea via the northern entrance of Ombai; however, it is difficult to test this hypothesis due to only XCTD data being recorded in this area with no dissolved oxygen measurements. Relatively salty North Indian Intermediate Water (NIIW) with a near surface density value of 27 σ_θ (blue-violet color in Fig. 7a) predominantly occupies the area around the southern Lesser Sunda Islands, associated with a minimum in dissolved oxygen content (Fieux et al., 2005).

At surface density values between 26.5 and 27.0 σ_θ, slightly saltier water is found in Banda than that observed in Ombai. This may be salty lower thermocline water (SPSLTW) found between 25.0 σ_θ and 26.0 σ_θ in Halmahera, that experienced downwelling by vertical mixing in Halmahera, Seram and the Manipa Straits. This could potentially also be the signature of salty North Indian Intermediate Water (NIIW), advected through Ombai into Banda, as suggested by Wyrtki (1961). During the

INDOMIX cruise, the intrusion of NIIW into Ombai was not observed; this salty water disappears at the station just before Ombai. The western and eastern side of the 25 km wide Ombai strait display different water masses, which suggests two branches of circulation: one coming from the Flores Sea with fresher water, and the other from saltier Banda water. In the upper thermocline layer (density of 23.5 σ_θ), a salinity difference of about 0.2 psu is observed.

f) Evidence of water mass intrusion from Indian/ Savu oxygen minimum water

A complementary XCTD sampling along the southern Lesser Sunda Arc was devoted to investigating the existence of salinity maximum North Indian Intermediate Water (NIIW) with low dissolved oxygen in the northern Savu Sea, which remains poorly constrained. Sprintall et al. (2009) observed eastward mean flow from INSTANT data and revealed two distinct current structures representing eastward South Java Current (SJC) near the sea surface, and South Java Under Current (SJUC) below thermocline depths, with a possible supply of Indian water into the region. In addition, Atmadipoera et al. (2009) found a weak signature of salty water in the intermediate layer in Ombai, considered as potentially NIIW in origin.

During the survey time, in the peak of the southeast monsoon season, the salinity maximum NIIW was strongly attenuated in the last two stations closest to Ombai, possibly due to the effects of the strong southwestward Ombai Throughflow that prevents its extension to the east and to the northern entrance of Ombai (see Section 3.1). Sprintall et al. (2009) showed that seasonal SJC and SJUC in Ombai Strait are fully developed during the two monsoon transitions. Thus, the observed NIIW during the peak southeast monsoon period may indicate that, to a great extent, the existence of the NIIW in the southern Lesser Sunda Arc is persistent, which corroborates eastward

mean flow in Ombai (Sprintall et al., 2009). There were no oxygen measurements taken along the Lesser Sunda Arc section, but previous studies (e.g., Fieux et al., 1994; Molcard et al., 2001) show that the NIIW is associated with low oxygen content (<90 μmol kg^{-1} or < 2 ml l^{-1}) because its oxygen content is biologically consumed and as a result of weak circulation in its source water mass in the Red Sea (Fieux et al., 2005, 1994; Rochford, 1965; Wyrtki, 1961).

During the cruise the extension of NIIW water is blocked by strong southwestward throughflow when approaching the Ombai Strait. Observation of NIIW recirculation within the Savu Sea and its possible intrusion into Banda Sea via the northern and eastern portal of the Ombai Strait are still a challenge. However, recent model study suggested that a reversal throughflow via Ombai Strait brings Indian intermediate water into interior seas and farther into the western tropical Pacific Ocean (Liang et al., 2020).

4. CONCLUSIONS

The INDOMIX cruise, carried out in July 2010, provides a unique dataset to document water masses and currents along the track from the edge of the Pacific Ocean to the Halmahera entry portal to the southern Lesser Sunda Arc, successively crossing the Seram Sea, Manipa Strait, Banda Sea, Ombai Strait, northern Savu Sea, Sumba Strait, and south of Lombok Strait. We observed various water masses of Northern and Southern Pacific Water origin within the ITF region, as well as local near-surface fresh water, and Indian water origin. In previous studies, hydrographic data in these regions was rare and had not been acquired during the same time period. For the first time, the INDOMIX cruise provides a synoptic overview of water mass transformation along the

eastern path of the ITF. A contrast of water masses between much fresher and colder thermocline ITF water, derived from the western ITF route, and warmer, salty ITF water from the eastern ITF path was recorded during the cruise. The fresh and colder thermocline water found in Banda and Ombai is the characteristic of a salty NPSW origin, freshened by surface Java Sea water through the vertical mixing en route in the Flores Sea, whereas much saltier and warmer thermocline water, typical of SPSW origin, is confined to the Halmahera Sea and part of the Seram Sea. A sharp front between both water masses occurs in Seram Sea, where a drastic extinction of SPSW salinity is recorded, which is likely related to partitioning of the flows, and strong vertical mixing induced by internal tides, as observed during the cruise.

The southward flow of ITF in Halmahera Sea was revealed by both the shipboard and lowered ADCP. The 24-hour stations in the Halmahera Sea and the Ombai Strait allow characterization of the dynamics of the currents. These currents are dominated by a strong tidal signal, both barotropic and baroclinic, that was inferred from different stations over two M2 tidal cycles. The diurnal component dominates the barotropic current in the northern study area (stations C1, C2, and C3) and the semidiurnal components dominate in the southern part (station C5), while both diurnal and semidiurnal baroclinic tides of the same order of magnitude are observed at all stations. Moreover, the observed currents reveal the northward flow in the Manipa Strait, a feature not previously described in ITF circulation. This flow may originate from local recirculation, and bring local water mass from Banda to the Seram Sea; further study is needed to quantify the water mass transport in those straits and its variability. It is also found the southward flows in the secondary outflow portals in the Alas and Sape Straits (located in the Lesser Sunda Arc).

Large extinction of South Pacific water origin in the Halmahera Sea is associated with strong vertical mixing process forced by the internal tidal activities. Here, by employing the INDOMIX dissipation rate and vertical diffusivity data from the VMP, a simplified advection/diffusion model demonstrated successfully the transformation of salty Pacific thermocline water in several days from the entry portal to the exit passage in the Halmahera Sea.

Salty South Pacific Subtropical Water is strongly eroded when entering the Halmahera Sea, losing its salinity by about 0.5 psu in a lateral distance of less than 250 km between the Pacific (station C0) and the exit portal of Halmahera (station C3), as a consequence of substantial mixing taking place in the rather short distance between C1 and C3 (20 km). We found, that the 24-hour CTD "yoyo" station, where several CTD casts have been collected, allows the identification of large isopycnal vertical displacements. Large vertical fluctuation of isotherms may express strong internal tidal activity in the region, as also noted in Koch-Larrouy et al. (2015) and Nugroho et al. (2018), where isopycnal displacements were found in the INDOMIX data and the INDESO model to be as large as 40 m in magnitude.

Using velocity and Kz (Koch-Larrouy et al., 2015) values measured at C1, C2, and C3 during the cruise, we use a simple advection/diffusion equation to account for the mean vertical profiles of heat and salinity, given the vertical distribution at station C0. The results show that vertical mixing is the dominant process in the Halmahera sea which explains the transformation of Pacific Water (station C0 profile) into homogeneous Halmahera water within 2 days of Kz1 and 1 day of Kz3. After 4 days, the results remain almost unchanged suggesting a minimum energy threshold is required to thoroughly mix the Halmahera water mass (not shown). This result deduced

from the observations measurements is in good agreement with the modeling results of Nagai et al. (2017) and Nugroho et al. (2016).

The salinity maximum of SPSW at site C2 on certain surface density values (for example, 24.7, 25.4, and 26.0 σ_θ) is higher than that observed in the entry portals (C1). This could be explained by the fact that C1 may not be the only route of the source water filling site C2 and that the mixing at C1 is very strong. In addition, this could also be due to a large degree of variability in the current system, comprising the New Guinea Coastal/Undercurrent and the Halmahera Eddy that could supply different sources of water masses (e.g., mixed salty SPSW and NPSW) that are advected into the Halmahera Sea (Kashino et al., 2013).

Evidence of the inter-leaving of SPSW water between the thermocline and intermediate layer is found in the central Halmahera basin. This feature may be related to lateral advection processes, where the new arrival of SPSW water is advected by throughflow into 'older' existing water mass, since zigzagged T-S profiles here overlay those observed at the entry portal of Halmahera. We found in this paper that stronger interleaving features are seen at sites C0 and C2, compared to sites C1 and C3. This can be interpreted as follow: at C1 and C3 where very strong vertical mixing has been found (Koch-Larrouy et al. 2015) homogenizes these instabilities making them disappear, in contrast to C2 where much smaller vertical diffusivities are found. This lateral process might favor instabilities that concur in the well mixed Halmahera water mass as also suggested by Nagai et al. (2017) and Nagai et al. (2021).

New insight into the presence of salty North Indian Intermediate Water in the southern Lesser Sunda Arc section corroborates a persistent eastward South Java Undercurrent that is previously found in Ombai. However, during this study the intrusion of NIIW was not identified in Ombai, possibly because of strong

southwestward throughflow that may force the waters to recirculate within the Savu Sea. It is likely that during the transition monsoon period when the SJUC is much stronger (Sprintall et al 2009), NIIW water may be advected farther east into Banda via northern and eastern portals of the Ombai Strait. Finally, a field hydrographic measurement around the Ombai Strait is needed to approve this idea.

In a companion paper (Part II), the INDOMIX data for the biogeochemical properties are presented and used to analyze the impact of internal tides on the nutrients and chlorophyll concentrations, and potentially the primary production in the eastern Indonesian region.

ACKNOWLEDGMENTS

The INDOMIX cruise is a collaborative research effort between France and Indonesia. We would like to warmly thank the IPB vice-rector for research and cooperation for the cruise organization. We thank the *Institute Polaire Français Paul-Emil-Victor* (IPEV), who provided the Marion Dufresne for the cruise. We are grateful to Dr. Hélène Leau from IPEV, the captain and crew of R.V. Marion Dufresne for their support during the cruise. This work was supported by LEFE-IDAO/INSU and additional funding by LEGOS and IRD. The vertical microstructure profiler (VMP) was funded by the *French Agence Nationale de la Recherche* (ANR) through the ANR-JC05-50690 grant and part of the functioning expenses by the French Institute for Marine Science (IFREMER). DT-INSU provided the CTD. Claudie Marec and Annie Kartavtseff helped with calibrating CTD and processing SADCP data using CODAS 3. Visits of Indonesian scientists in France and French scientists in Indonesia to prepare the cruise and analyze the data were supported by IRD (SELTAR project) and *Institute Français in Indonesia* (IFI). We also acknowledge support and assistance from the IRD Best program, and

IRD Jakarta representative and the French Embassy in Jakarta, the Ministry of Education National of Indonesia, and the Ministry of Research and Technology. ASA was funded in part by a grant from the Ministry Education National (DIKTI) Indonesia, through contracts no. 591.11/I 3/11/P L/2011 and no. 591.11/I 3/11/P L/2012. The authors gratefully thank and sincerely appreciate two anonymous reviewers for their constructive comments and suggestions, which helped us to improve the quality of manuscript.

REFERENCES

Ando, K., Hasegawa, T., 2009. Annual zonal displacement of Pacific warm pool in association with El Niño onset. Sci. Online Lett. Atmos. 5, 149–152. https://doi.org/10.2151/sola.2009-038

Atmadipoera, A., Molcard, R., Madec, G., Wijffels, S., Sprintall, J., Koch-Larrouy, A., Jaya, I., Supangat, A., 2009. Characteristics and variability of the Indonesian throughflow water at the outflow straits. Deep. Res. Part I Oceanogr. Res. Pap. 56. https://doi.org/10.1016/j.dsr.2009.06.004

Bourdallé-Badie, R., Bell, M., Chanut, J., Clementi, E., Coward, A., Drudi, M., Éthé, C., Iovino, D., Lea, D., Lévy, C., Madec, G., Martin, N., Masson, S., Mathiot, P., Mocavero, S., Müller, S., Nurser, G., Samson, G., Storkey, D., 2019. "NEMO ocean engine", Scientific Notes of Climate Modelling Center, 27 — ISSN 1288-1619, Institut Pierre-Simon Laplace (IPSL), doi:10.5281/zenodo.1464816.

Bouruet-Aubertot, P., Cuypers, Y., Ferron, B., Dausse, D., Ménage, O., Atmadipoera, A., Jaya, I., 2018. Contrasted turbulence intensities in the Indonesian Throughflow: a challenge for parameterizing energy dissipation rate. Ocean Dyn. 68. https://doi.org/10.1007/s10236-018-1159-3

Broecker, W.S., Patzert, W.C., Toggweiler, J.R., Stuiver, M., 1986. Hydrography, chemistry, and radioisotopes in the Southeast Asian basins. J. Geophys. Res. https://doi.org/10.1029/jc091ic12p14345

Buijsman, M.C., Ansong, J.K., Arbic, B.K., Richman, J.G., Shriver, J.F., Timko, P.G., Wallcraft, A.J., Whalen, C.B., Zhao, Z., 2016. Impact of parameterized internal wave drag on the semidiurnal energy balance in a global ocean circulation model. J. Phys. Oceanogr. 46, 1399–1419. https://doi.org/10.1175/JPO-D-15-0074.1

Cresswell, G., Frische, A., Peterson, J., Quadfasel, D., 1993. Circulation in the Timor Sea. J. Geophys. Res. Ocean. 98, 14379–14389. https://doi.org/10.1029/93jc00317.

Dillon, T.M., 1982. Vertical overturns: A comparison of Thorpe and Ozmidov length scales. J. Geophys. Res. https://doi.org/10.1029/jc087ic12p09601

Fang, G., Susanto, R.D., Wirasantosa, S., Qiao, F., Supangat, A., Fan, B., Wei, Z., Sulistiyo, B., Li, S., 2010. Volume, heat, and freshwater transports from the South China Sea to Indonesian seas in the boreal winter of 2007-2008. J. Geophys. Res. Ocean. 115, 1–11. https://doi.org/10.1029/2010JC006225

Ffield, A., Gordon, A.L., 1992. Vertical Mixing in the Indonesian Thermocline. J. Phys. Oceanogr. https://doi.org/10.1175/1520-0485(1992)022<0184:VMITIT>2.0.CO;2

Ffield, A., Robertson, R., 2005. Indonesian Seas Finestructure Variability. Oceanography 18, 108–111. https://doi.org/10.5670/oceanog.2005.11

Fieux, M., Andrié, C., Delecluse, P., Ilahude, A.G., Kartavtseff, A., Mantisi, F., Molcard, R., Swallow, J.C., 1994. Measurements within the Pacific-Indian oceans throughflow region. Deep Sea Res. Part I Oceanogr. Res. Pap. 41, 1091–1130. https://doi.org/10.1016/0967-0637(94)90020-5

Fieux, M., Molcard, R., Morrow, R., Kartavtseff, A., Ilahude, A.G., 2005. Variability of the throughflow at its exit in the Indian Ocean. Geophys. Res. Lett. 32, 1–4. https://doi.org/10.1029/2005GL022836

Firing, E., Ranada, J., Caldwell, P., 1995. Processing ADCP Data With the Codas Software System Version 3.1 226.

Fischer, J., Visbeck, M., 1993. Deep velocity profiling with self-contained ADCPs. J. Atmos. Ocean. Technol. https://doi.org/10.1175/1520-0426(1993)010<0764:DVPWSC>2.0.CO;2

Geary, J.E., 2012. The effect of wind upon the mixed-layer depth., The effect of wind upon the mixed-layer depth. https://doi.org/10.5962/bhl.title.58734

Godfrey, J.S., 1996. The effect of the Indonesian throughflow on ocean circulation and heat exchange with the atmosphere: A review. J. Geophys. Res. 101, 12217. https://doi.org/10.1029/95JC03860

Gordon, A., 2005. Oceanography of the Indonesian Seas. Oceanography 18, 14–27. https://doi.org/10.5670/oceanog.2005.18

Gordon, A.L., 1986. Inter-ocean exchange of thermohaline water. J. Geophys. Res. 91, 5037–5046.

Gordon, A.L., Fine, R.A., 1996. Pathways of water between the Pacific and Indian oceans in the Indonesian seas. Nature 379, 146–149. https://doi.org/10.1038/379146a0

Gordon, A.L., Giulivi, C.F., Ilahude, A. G., 2003. Deep topographic barriers within the Indonesian seas. Deep. Res. Part II Top. Stud. Oceanogr. 50, 2205–2228. https://doi.org/10.1016/S0967-0645(03)00053-5

Gordon, A.L., Sprintall, J., Van Aken, H.M., Susanto, D., Wijffels, S., Molcard, R., Ffield, A., Pranowo, W., Wirasantosa, S., 2010. The Indonesian throughflow

during 2004-2006 as observed by the INSTANT program. Dyn. Atmos. Ocean. 50, 115–128. https://doi.org/10.1016/j.dynatmoce.2009.12.002

Gordon, A.L., Susanto, R.D., Ffield, A., Huber, B.A., Pranowo, W., Wirasantosa, S., 2008. Makassar Strait throughflow, 2004 to 2006. Geophys. Res. Lett. 35, 3–7. https://doi.org/10.1029/2008GL036372

Hatayama, T., 2004. Transformation of the Indonesian throughflow water by vertical mixing and its relation to tidally generated internal waves. J. Oceanogr. 60, 569–585. https://doi.org/Doi 10.1023/B:Joce.0000038350.32155.Cb

Hautala, S.L., Reid, J.L., Bray, N., 1996. The distribution and mixing of the Pacific water masses in the Indonesian Seas. J. Geophys. Res. Ocean. 101 (C5), 12375–12389. https://doi.org/10.1029/96JC00037.

Ilahude, A.G., Gordon, A.L., 1996. Thermocline stratification within the Indonesian Seas. J. Geophys. Res. https://doi.org/10.1029/95JC03798

Kara, A.B., Rochford, P.A., Hurlburt, H.E., 2003. Mixed layer depth variability over the global ocean. J. Geophys. Res. Ocean. 108, 1–15. https://doi.org/10.1029/2000jc000736.

Kashino, Y., Aoyama, M., Kawano, T., Hendiarti, N., Syaefudin, Anantasena, Y., Muneyama, K., Watanabe, H., 1996. The water masses between Mindanao and New Guinea. J. Geophys. Res. Ocean. 101, 12391-12400. https://doi.org/10.1029/95JC03797

Kashino, Y., Atmadipoera, A., Kuroda, Y., Lukijanto, 2013. Observed features of the Halmahera and Mindanao Eddies. J. Geophys. Res. Ocean. 118, 6543–6560. https://doi.org/10.1002/2013JC009207

Kashino, Y., Ueki, I., Sasaki, H., 2015. Ocean variability east of Mindanao: Mooring observations at 7°N, revisited. J. Geopysical Res. Ocean. 2540–2554.

https://doi.org/10.1002/2015JC010703.Received

Koch-Larrouy, A., Atmadipoera, A., van Beek, P., Madec, G., Aucan, J., Lyard, F., Grelet, J., Souhaut, M., 2015. Estimates of tidal mixing in the Indonesian archipelago from multidisciplinary INDOMIX in-situ data. Deep Sea Res. Part I Oceanogr. Res. Pap. 106, 136–153. https://doi.org/10.1016/j.dsr.2015.09.007

Koch-Larrouy, A., Madec, G., Bouruet-Aubertot, P., Gerkema, T., Bessières, L., Molcard, R., 2007. On the transformation of Pacific Water into Indonesian Throughflow Water by internal tidal mixing. Geophys. Res. Lett. 34, L04604. https://doi.org/10.1029/2006GL028405

Koch-Larrouy, A., Madec, G., Iudicone, D., Atmadipoera, A., Molcard, R., 2008. Physical processes contributing to the water mass transformation of the Indonesian throughflow. Ocean Dyn. 58. https://doi.org/10.1007/s10236-008-0154-5

Kuroda, Y., 2000. Variability of currents off the northern coast of New Guinea. J. Oceanogr., 56, 103–116. https://doi.org/10.1023/A:1011122810354

Li, X., Yuan, D., Wang, Z., Li, Y., Corvianawatie, C., Surinati, D., Sandra, A., Bayhaqi, A., Avianto, P., Kusmanto, E., Dirhamsyah, D., Arifin Z., 2020. Moored observation of transport and variability of Halmahera Sea currents. J. Phys. Oceanogr. 50, 471-488. https://doi.org/ 10.1175/JPO-D-19-0109.1.

Liang, L., Xue, H., & Shu, Y. (2019). The Indonesian throughflow and the circulation in the Banda Sea: A modeling study. J. of Geophys. Res.: Oceans, 124, 3089–3106. https://doi.org/10.1029/2018JC014926.

Liang, L., and Xue, H. 2020. The reversal Indian Ocean waters. Geophys. Res. Lett. 47 (14), e2020GL088269. https://doi.org/10.1029/2020GL088269.

Luick, J.L., Cresswell, G.R., 2001. Current measurements in the Maluku Sea. J. Geophys. Res. Ocean. 106, 13953–13958. https://doi.org/10.1029/2000jc000694

Lukas, R., Lindstrom, E., 1991. The mixed layer of the western equatorial Pacific Ocean. J. Geophys. Res. Ocean. 96, 3343–3357. https://doi.org/doi:10.1029/90JC01951

Madec, G., and the NEMO team, 2014. NEMO ocean engine. *Note du Pôle de modélisation*, Institut Pierre-Simon Laplace (IPSL), France, No 27, ISSN No 1288-1619. https://www.nemo-ocean.eu/doc/.

Meyers, G., 1996. Variation of Indonesian throughflow and the El Niño-Southern Oscillation. J. Geophys. Res. 101 (C5), 12255-12263. https://doi.org/10.1029/95JC03729

Molcard, R., Fieux, M., Ilahude, A. G., 1996. The Indo-Pacific throughflow in the Timor Passage. J. Geophys. Res. 101, 12411. https://doi.org/10.1029/95JC03565

Molcard, R., Fieux, M., Syamsudin, F., 2001. The throughflow within Ombai Strait. Deep. Res. Part I Oceanogr. Res. Pap. 48(6). https://doi.org/10.1016/S0967-0637(00)00084-4

Nagai, T., Hibiya, T., & Bouruet-Aubertot, P., 2017. Nonhydrostatic simulations of tide-induced mixing in the Halmahera Sea: A possible role in the transformation of the Indonesian Throughflow waters. J. of Geophys. Res. Ocean. 122,8933–8943. https://doi.org/10.1002/2017JC013381

Nagai, T., Hibiya, T., Syamsudin F., 2021. Direct Estimates of turbulent mixing in the Indonesian Archipelago and its role in the transformation of the Indonesian Throughflow Waters. Geophys. Res. Lett. 48, e2020GL091731. https://doi.org/10.1029/2020GL091731

Nugroho, D., Koch-Larrouy, A., Gaspar, P., Lyard, F., Reffray, G., Tranchant, B., 2017. Modelling explicit tides in the Indonesian seas: An important process for surface sea water properties. Mar. Pollut. Bull.

https://doi.org/10.1016/j.marpolbul.2017.06.033

Potemra, J.T., 2003. Observed estimates of convergence in the Savu Sea, Indonesia. J. Geophys. Res. 108, 1–11. https://doi.org/10.1029/2002JC001507

Purwandana, A., Cuypers, Y., Bouruet-Aubertot, P., Nagai, T., Hibiya, T., Atmadipoera, A.S., 2020. Spatial structure of turbulent mixing inferred from historical CTD datasets in the Indonesian seas. Prog. Oceanogr. 184, 102312. https://doi.org/10.1016/j.pocean.2020.102312

Robertson, R., 2010. Interactions between tides and other frequencies in the Indonesian seas. Ocean Dyn. 61, 69–88. https://doi.org/10.1007/s10236-010-0343-x

Rochford, D.J., 1965. Distribution of Banda intermediate water in the Indian Ocean. Mar. Freshw. Res. https://doi.org/10.1071/MF9660061

Sloyan, B.M., Talley, L.D., Chereskin, T.K., Fine, R., Holte, J., 2010. Antarctic Intermediate Water and Subantarctic Mode Water Formation in the Southeast Pacific: The Role of Turbulent Mixing. J. Phys. Oceanogr. 40 (7), 1558-1574. https://doi.org/10.1175/2010JPO4114.1

Sprintall, J., Gordon, A.L., Koch-Larrouy, A., Lee, T., Potemra, J.T., Pujiana, K., Wijffels, S.E., 2014. The Indonesian seas and their role in the coupled ocean–climate system. Nat. Geosci. 7, 487–492. https://doi.org/10.1038/ngeo2188

Sprintall, J., Gordon, A.L., Wijffels, S.E., Feng, M., Hu, S., Koch-Larrouy, A., Phillips, H., Nugroho, D., Napitu, A., Pujiana, K., Dwi Susanto, R., Sloyan, B., Yuan, D., Riama, N.F., Siswanto, S., Kuswardani, A., Arifin, Z., Wahyudi, A.J., Zhou, H., Nagai, T., Ansong, J.K., Bourdalle-Badié, R., Chanut, J., Lyard, F., Arbic, B.K., Ramdhani, A., Setiawan, A., 2019. Detecting change in the Indonesian seas. Front. Mar. Sci. 6. https://doi.org/10.3389/fmars.2019.00257

Sprintall, J., Potemra, J.T., Hautala, S.L., Bray, N.A., Pandoe, W.W., 2003.

Temperature and salinity variability in the exit passages of the Indonesian Throughflow. Deep. Res. Part II Top. Stud. Oceanogr. 50, 2183–2204. https://doi.org/10.1016/S0967-0645(03)00052-3

Sprintall, J., Wijffels, S., Molcard, R., Jaya, I., 2010. Direct evidence of the South Java Current system in Ombai Strait. Dyn. Atmos. Ocean. 50, 140–156. https://doi.org/10.1016/j.dynatmoce.2010.02.006

Sprintall, J., Wijffels, S.E., Molcard, R., Jaya, I., 2009. Direct estimates of the indonesian throughflow entering the indian ocean: 2004-2006. J. Geophys. Res. Ocean. 114, 2004–2006. https://doi.org/10.1029/2008JC005257

Syamsudin, F., van Aken, H.M., Kaneko, A., 2010. Annual variation of the southern boundary current in the Banda Sea. Dyn. Atmos. Ocean. 50, 129–139. https://doi.org/10.1016/j.dynatmoce.2009.12.005

Talley, L.D., Sprintall, J., 2005. Deep expression of the Indonesian Throughflow: Indonesian Intermediate Water in the South Equatorial Current. J. Geophys. Res. C Ocean. 110, 1–30. https://doi.org/10.1029/2004JC002826

Tanguy, Y., Arnault, S., Lattes, P., 2010. Isothermal, mixed, and barrier layers in the subtropical and tropical Atlantic Ocean during the ARAMIS experiment. Deep. Res. Part I Oceanogr. Res. Pap. 57, 501–517. https://doi.org/10.1016/j.dsr.2009.12.012

Thurnherr, A., 2011. How to process LADCP data with the LDEO software. version IX 1–32.

Tranchant, B., Reffray, G., Greiner, E., Nugroho, D., Saint-agne, R., Saint-agne, R., 2015. Evaluation of an operational ocean model configuration at 1/12° spatial resolution for the Indonesian seas. Part I : ocean physics 1–49. https://doi.org/10.5194/gmdd-8-6669-2015

Van Aken, H.M., Brodjonegoro, I.S., Jaya, I., 2009. The deep-water motion through the Lifamatola Passage and its contribution to the Indonesian throughflow. Deep Sea Res. Part I Oceanogr. Res. Pap. 56, 1203–1216. https://doi.org/10.1016/j.dsr.2009.02.001

Van Aken, H.M., Punjanan, J., Saimima, S., 1988. Physical aspects of the flushing of the east Indonesian basins. Netherlands J. Sea Res. 22, 315–339. https://doi.org/http://dx.doi.org/10.1016/0077-7579(88)90003-8

Visbeck, M., 2002. Deep velocity profiling using lowered acoustic Doppler current profilers: Bottom track and inverse solutions. J. Atmos. Ocean. Technol. 19, 794–807. https://doi.org/10.1175/1520-0426(2002)019<0794:DVPULA>2.0.CO

Wang, B., Huang, F., Wu, Z., Yang, J., Fu, X., Kikuchi, K., 2009. Multi-scale climate variability of the South China Sea monsoon: A review. Dyn. Atmos. Ocean. 47, 15–37. https://doi.org/10.1016/j.dynatmoce.2008.09.004

Wen, X., Peng, S., Qian, Y-K., Li, Y., 2021. Diversity in Vertical Structures of Internal Tide Dissipation Rate Around the Indonesian Throughflow Exits Simulated by a High-Resolution Nonhydrostatic Model. Geophys. Res. Lett. 48, e2021GL092706. https://doi.org/10.1029/2021GL092706

Wijffels, S., Sprintall, J., Fieux, M., Bray, N., 2002. The JADE and WOCE I10/IR6 throughfow sections in the southeast Indian Ocean. Part 1: water mass distribution and variability. Deep-Sea Research Part II: Top. Stud. Oceanogr. 49, 1341–1362.

Wyrtki, K., 1961. Physical Oceanography of the Southeast Asian Waters. NAGA Rep. Vol.2, Sci. Results Mar. Investig. South China Sea Gulf Thail. 1951-1961 2. https://doi.org/10.1017/S0025315400054370.

Zhu, Y., Wang, L., Wang, Y., Xu, T.,Li, S., Cao, G., et al. (2019). Stratified circulation in the Banda Sea and its causal mechanism. J. of Geophys. Res.: Oceans,

124.https://doi.org/10.1029/2019JC015279

1 Tables Captions

2 **Table 1**. Description of CTD-O and XCTD stations measurements during the INDOMIX experiment

No.	Date	Stat.	Geographical Position	Number of casts	Bottom depth (m)	Instrument depth of each profile (m)
1.	10-Jul-2010-18:57 10-Jul-2010-20:02	C0	129.985°E; 0.969°N	2	3050	104-3020
2.	11-Jul-2010-09:48 12-Jul-2010-11:59	C1	129.174°E; 0.060°N	8	950	896-908-905-934- 950-936-935-937
3.	12-Jul-2010-16:07 13-Jul-2010-14:44	C2	128.883°E; 0.752°S	9	1450	1415-1418-1423- 1424-1421-1414- 1406-1403-1352
4.	13-Jul-2010-19:11 14-Jul-2010-17:46	C3	128.883°E; 1.135°S	12	900	894-884-895-898- 905-895-893-880- 891-904-905-914
5.	15-Jul-2010-21:56 16-Jul-2010-20:23	C4	126.998°E; 6.286°S	2	4500	502-4435

6.	16-Jul-2010-16:18 17-Jul-2010-14:09	C5	125.386°E; 8.250°S 125.244°E; 8.284°S	9	1550	1429-1491-1517- 1509-1181-409- 1549-1414-1303
7			XCTD Ceram			
	14-Jul-2010-23:47	X02	128.504°E; 1.55°S	1	1500	
	15-Jul-2010-02:03	X03	128.201°E; 2.04°S	1	2000	
	15-Jul-2010-04:00	X04	127.936°E; 2.46°S	1	3000	
	15-Jul-2010-05:53	X05	127.683°E; 2.86°S	1	1500	
	15-Jul-2010-08:30	X06	127.392°E; 3.40°S	1	2000	
8			XCTD Banda			
	15-Jul-2010-10:12	X07	127.336°E; 3.80°S	1	3700	
	15-Jul-2010-12:16	X08	127.284°E; 4.28°S	1	3700	
	15-Jul-2010-14:40	X09	127.208°E; 4.80°S	1	4000	
	15-Jul-2010-17:23	X10	127.118°E; 5.41°S	1	4200	
	16-Jul-2010-07:42	X11	126.605°E; 6.78°S	1	3800	
	16-Jul-2010-09:32	X12	126.300°E; 7.12°S	1	2500	
	16-Jul-2010-16:11	X13	125.970°E; 7.49°S	1	2000	
9			XCTD Small Sunda Arcs			
	17-Jul-2010-17:22	X15	124.822°E; 8.49°S	1	2000	

	17-Jul-2010-19:20	X16	124.195°E; 8.62°S	1	2000	
	17-Jul-2010-22:20	X17	123.603°E; 8.72°S	1	1800	
	18-Jul-2010-00:46	X18	122.958°E; 8.80°S	1	2000	
	18-Jul-2010-03:26	X19	122.230°E; 8.88°S	1	2300	
	18-Jul-2010-07:11	X20	121.342°E; 8.98°S	1	2200	
	18-Jul-2010-09:40	X21	121.319°E; 8.96°S	1	1900	
	18-Jul-2010-12:56	X22	119.896°E; 9.03°S	1	2100	
	18-Jul-2010-13:27	X23	119.782°E; 9.03°S	1	2000	
	18-Jul-2010-17:44	X25	118.707°E; 9.07°S	1	2300	
	18-Jul-2010-21:05	X26	117.912°E; 9.11°S	1	1900	

3

4

5

6 **Table 2**. The water masses characteristics in the study area, identified from the INDOMIX experiment

	C0 Pacific	C1 North Halmahera	C2 Central Halmahera	C3 South Halmahera	XCTD Ceram	XCTD Banda	C4 Banda	C5 Ombai	XCTD Savu	XCTD Sumba
Parameter	SURFACE WATER									
	C0	C1	C2	C3	XCTD Seram	XCTD Banda	C4	C5	XCTD Savu	XCTD Sumba
Potential Density Anomaly (kg/m3)	<22.0	<22.0	<22.0	<22.0	<22.0	<22.0	<22.0	<22.0	<22.0	<23.0
Potential.Temperature (°C)	28.62-29.69	28.28-29.79	28.24-29.72	28.46-29.54	25.57-28.75	27.87-28.26	27.31-28.05	26.55-28.48	26.20-27.04	23.82/23.36
Salinity (psu)	34.126-34.725	34.585-34.274	34.549-34.171	34.505-34.264	34.768-34.217	34.12-33.560 Large salinity variantion	33.956-33.992 Saltier at surface	33.794-33.396	33.706-33.610	34.071/33.888
Dissolved Oxygen (umol/kg)	158.116-187.23	166.244-188.921	168.472-189.281	171.034-188.189	-	-	160.776-191.004	174.990-190.756	-	-
Depth (m)	<90	56-132	34-82	29-62	42-73	51-69	63-85	44-115	38-98	51-58
	THERMOCLINE WATER									
	C0	C1	C2	C3	XCTD Seram	XCTD Banda	C4	C5	XCTD Savu	XCTD Sumba
	SPSW	SPSW	SPSW	SPSW	SPSW/SPSLTW	Banda Water	ITFW Banda Water	Banda/Flores water	Sawu Water/NIIW	Indian Water/NIIW
Potential Density Anomaly (kg/m3)	23.0 -25.0 D(Smax): 24.1	23.0-25.0 D(Smax): 23.719	23.0-25.0 D(Smax): 24.673 Interleaving	23.0-25.0 D(Smax) :23.399	23.0-25.0 23.879	23.0-25.0	23.0-25.0 Dens(Smax): 24.649	23.0-25.5	23.0-26.0	23.5-26.0
Potential Temperature (°C)	18.98-26.37 T(Smax): 23.0	25.88-19.05 T(Smax): 23.89	25.76-19.20 T(Smax): 20.37	25.85-18.55 T(Smax): 24.62	24.53-18.35 T(Smax): 22.81	24.74-	24.24-17.71 T(Smax): 19.16	23.83/24.23-17.66/17.09 T(Smax): 17.84	23.60-13.09 T(Smax): 15.14	22.27-13.15 T(Smax): 14.74

Salinity (psu)	35.028-34.979 SMax: 35.194	34.917-34.925 Smax (range): 34.896-35.054	34.885-34.908 Smax: 34.945-35.004	34.785-34.817 Smax: 34.919-34.848	34.770-34.756 Smax : 34.850-34.654	Smax34.582 Smin34.523 34.444/34.281	34.281-34.551 Smax: 34.552	34.093/34.408-34.529/34.453 Smax: 34.528	34.014-34.511 Smax: 34.527	34.159-34.523 Smax: 34.527
Dissolved Oxygen (umol/kg)	137.443-130.792 DO(Smax): 126.931 DOmax: 135.710 Depth:317	142.040-128.282 DO(Smax): 137.495-131.822	142.139-127.166 DO(Smax): 129.999	143.322-128.708 DO(Smax):139.706	-	-	138.924-127.478 DO(Smax): 123.643	159.317/153.870-133.205/129.696 DO(Smax): 133.808	-	-
Depth (m) Lower thermocline	215	181-227	206-232	198-243	170-220	146-159	155-162	194-215	192	177-203
	INTERMEDIATE/DEEP WATER									
	C0	C1	C2	C3	XCTD Seram	XCTD Banda	C4	C5	XCTD Savu	XCTD Sumba
	SPSLTW, AAIW, EqPW, AAIB	SPSLTW	SPSLTW	SPSLTW	SPSLTW, Banda water	Banda water	Banda water	Banda water	NIIW	NIIW
Potential Density Anomaly (kg/m3)	26.5-27.0 Deep: >27.0	26.5-27.0	26.5-27.0	26.5-27.0	26.5 – 27.0	26.5-27.0	26.5-27.0 Deep:	26.5-27.0	26.8-27.2	26.8-27.2
Potential Temperature (°C)	11.74-7.92 Deep :7.68-1.33	11.46-7.97	11.10-7.85	11.16-7.94	11.09/10.87 – 7.93/7.71	10.99/10.62 – 7.84/7.57	9.21-7.84	10.41	9.14-6.49 T(Smax): 8.90	9.17-6.52 T(Smax): 8.29
Salinity (psu)	34.859-34.596	34.749-34.624	34.674-34.623	34.679-34.632	34.662/34.609 – 34.632/34.591 Salty SPSLTW	34.637/34.552 – 34.618/34.581	34.577-34.583	34.514	34.616-34.625 Smax :34.697-34.702	34.624-34.630 Smax 34.703

	Deep : 34.584-34.673									
Dissolved Oxygen (umol/kg)	135.766-120.146 DOmin: 88.894 Depth:480m Deep: 116.028-140.873 DOmin: 93.847 Depth:949m	124.058-119.570	116.200-116.951 Slighty high DO: 122.316 Depth:530	117.870-114.601 Slighty high DO: 121.951 Depth:555	-	-	96.830 DOmin : 88.725 Depth : 502m	99.574 DOmin : 89.935 Depth :714	-	-

7

8

9

Figures Captions

Figure 1. Map of the study area of the INDOMIX cruise in the eastern Indonesian Archipelago. Bathymetry map is derived from the GEBCO with contour of 500 m, and every 1000 m interval. Red arrows denote a schematic flow of the Indonesian Throughflow (ITF). The southward Mindanao Current (MC) and the northwestward New Guinea Under Current (NGUC) bring North/South Pacific water, respectively. The clockwise Halmahera Eddy (HE) and the eastward North Equatorial Counter Current (NECC). Red dashed arrows represent seasonal surface flows in the Java Sea; the eastward flow of the South Java Coastal and Under Current along the southern Indonesian archipelago; and deep southward flow in the Maluku Sea. The circles represent various station measurements. The CTD-O/LADCP stations are named with C0 – C5. Inset (lower right) denotes the depth-distance section in the entry portal of Halmahera between Patani and Gebe, obtained from the multi-beam echo sounder.

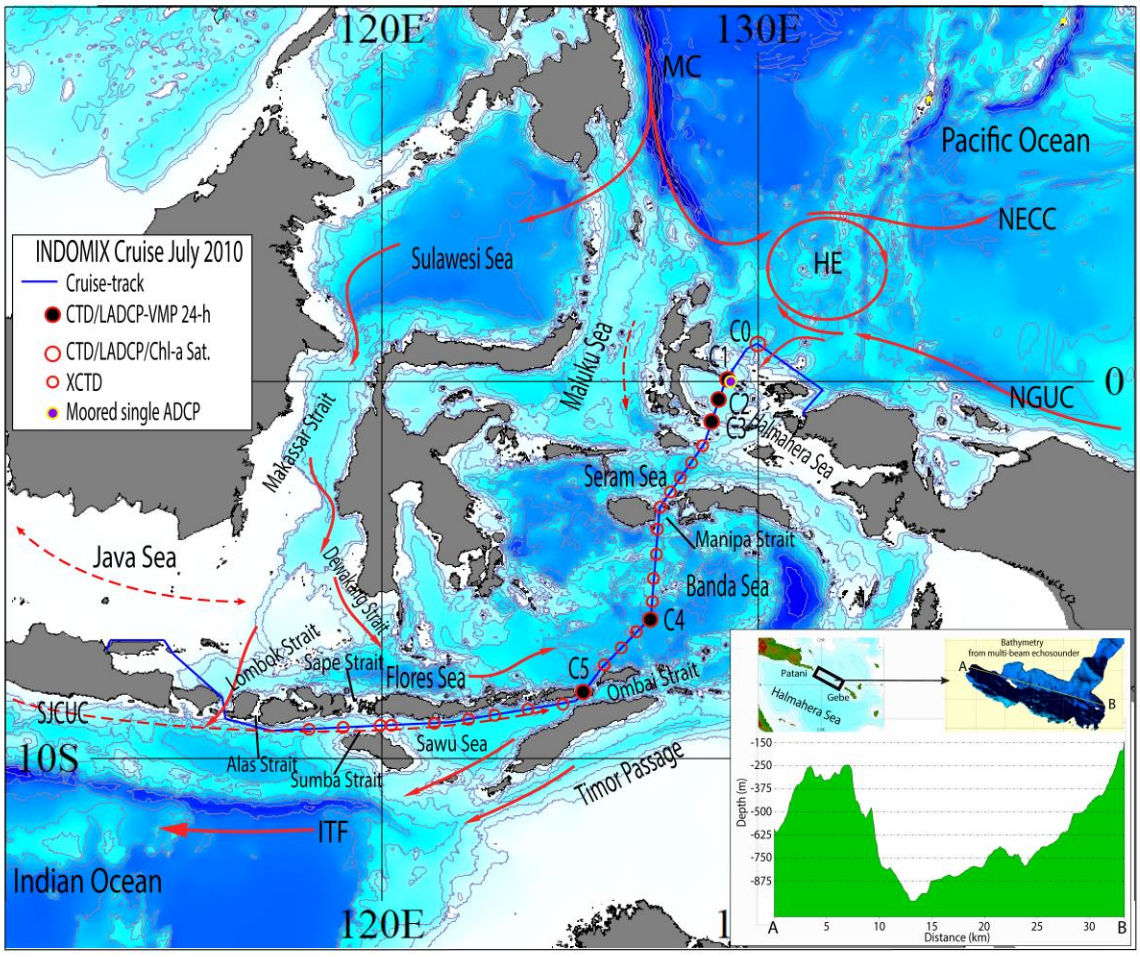

Figure 2. Averaged velocity vector between 20 m and 100 m depth (upper) and between 100 m and 200 m depth (lower) measured by the 150 kHz SADCP.

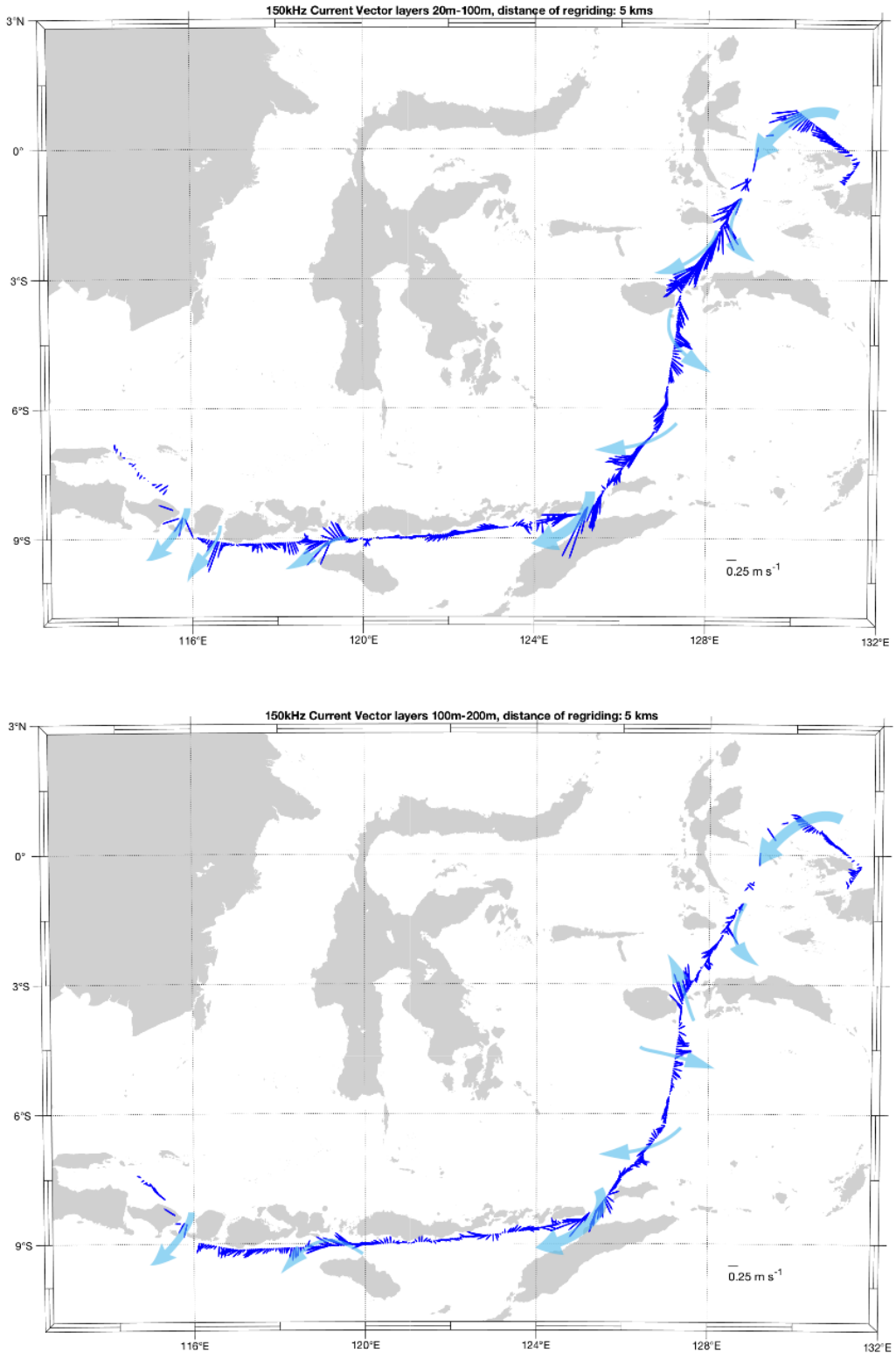

Figure 3. Distribution of (a) zonal and (b) meridional current from lowered ADCP for one tidal period (~24 hours); (c) the mean profiles of current components; and (d) zonal and (e) meridional distribution of baroclinic current in station C1.

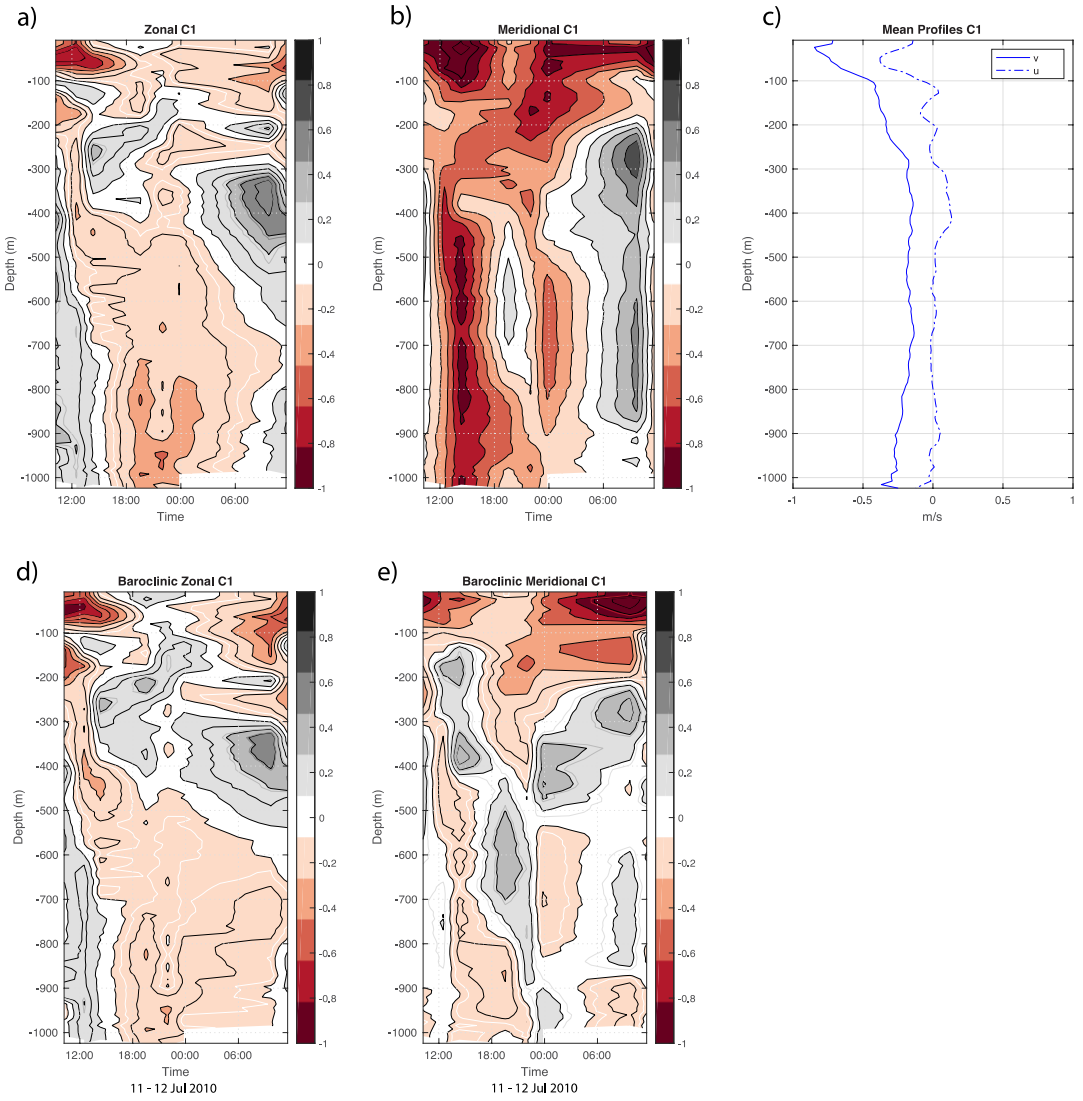

Figure 4. Same as Fig.3, but for station C2.

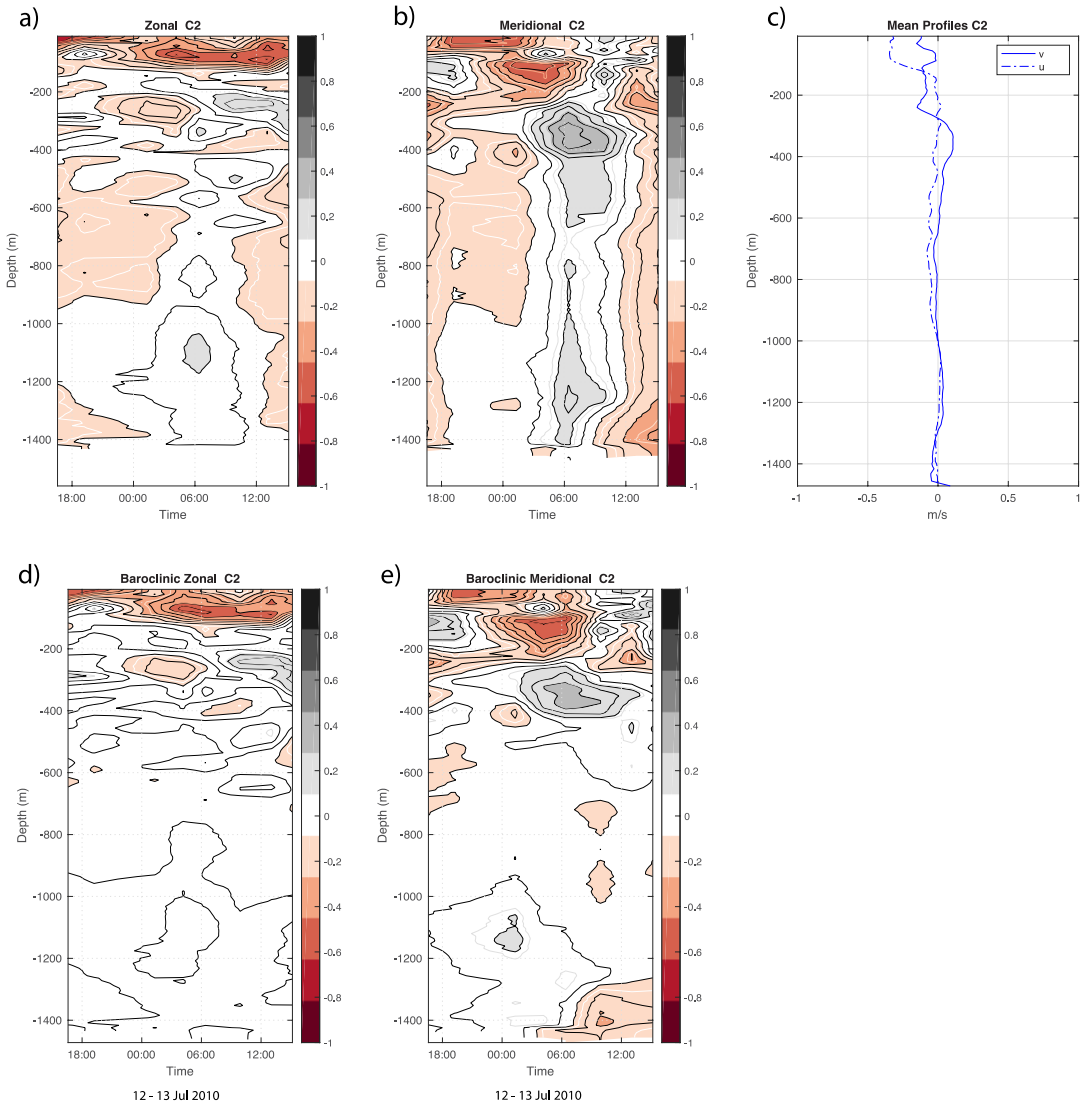

Figure 5. Same as Fig.3, but for station C3.

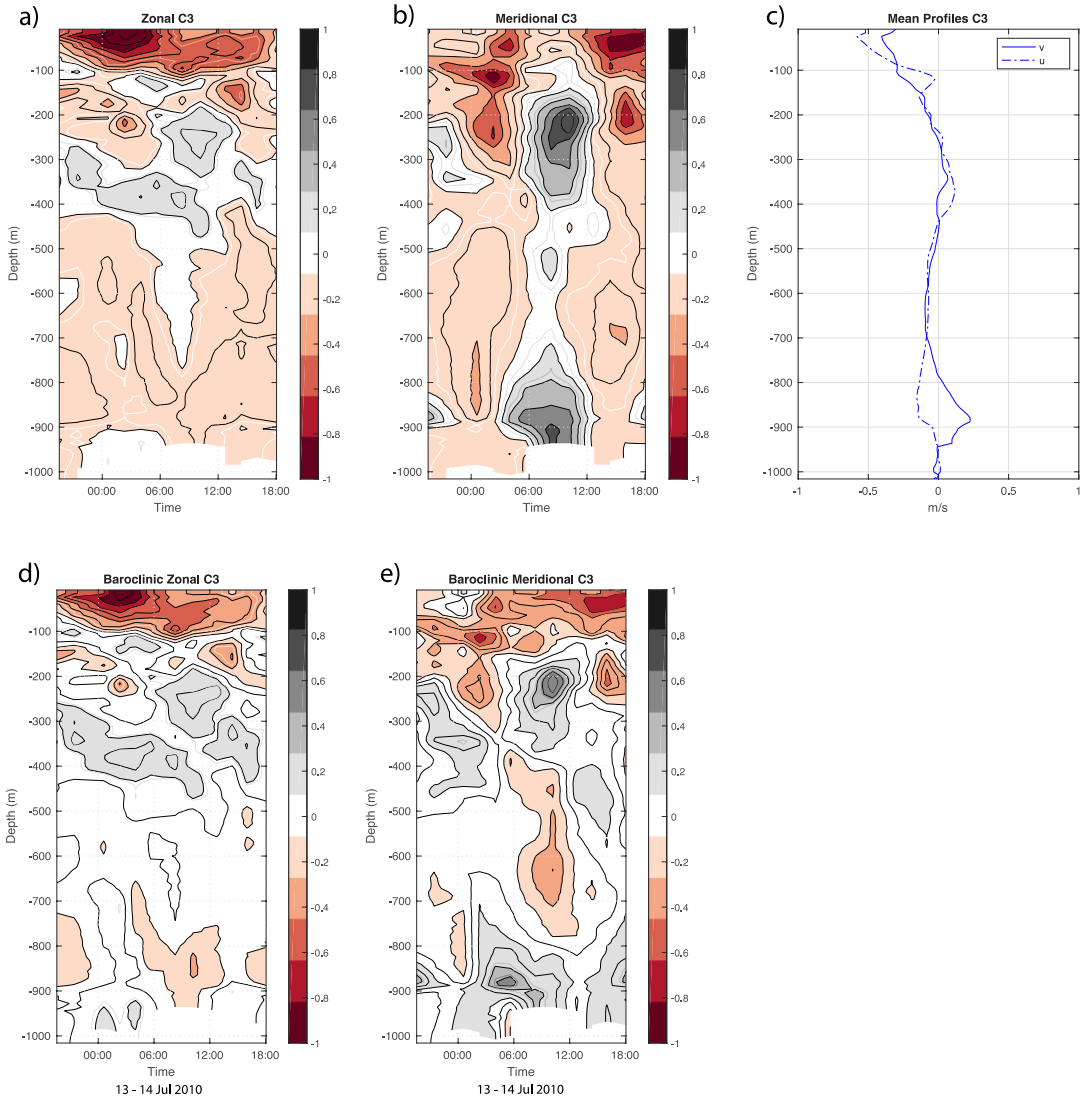

Figure 6. Same as Fig.3, but for station C5.

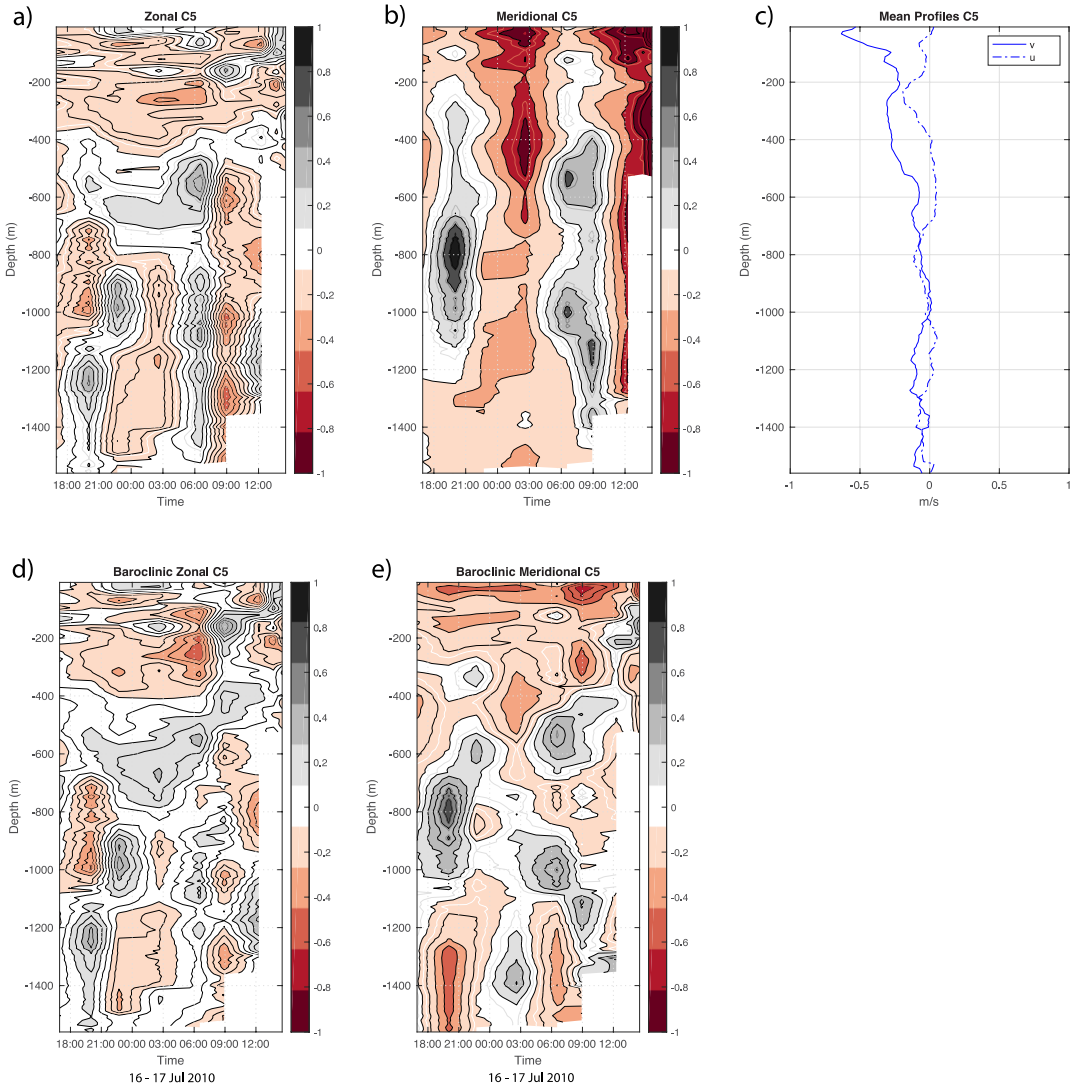

Figure 7. Diagram of (a) Temperature-Salinity, (b) Temperature-Dissolved Oxygen, and (c) Salinity-Dissolved Oxygen in the Pacific station (black), in the Halmahera Sea (dark red, red, orange), in the Ceram Sea (yellow), in the Manipa passage (light green), in the Banda Sea (green), in the Ombai Strait (light blue), and in the southern Lesser Sunda Islands (dark blue - violet). Insert shows the station positions along the cruise track. Note: no oxygen measurements in XCTD stations, such in Seram, north and south Banda, and southern Lesser Sunda Islands (see Fig.1 for reference of location).

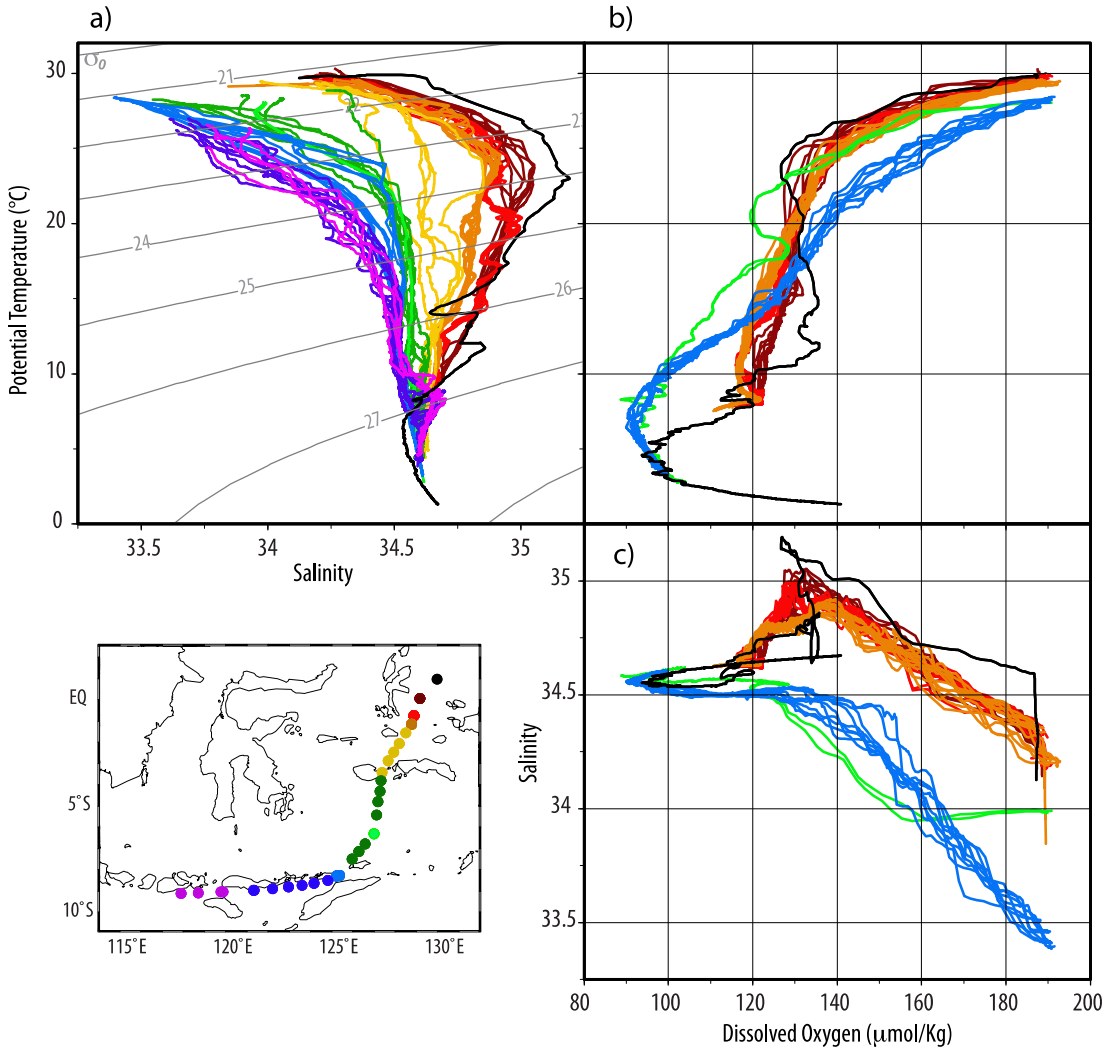

Figure 8. Potential Temperature section in the upper 1500 m along the cruise-track. Note the different depth scale. The horizontal axis denotes the survey date, corresponding to survey location (see Fig.1). Upper-outer ticks represent station positions.

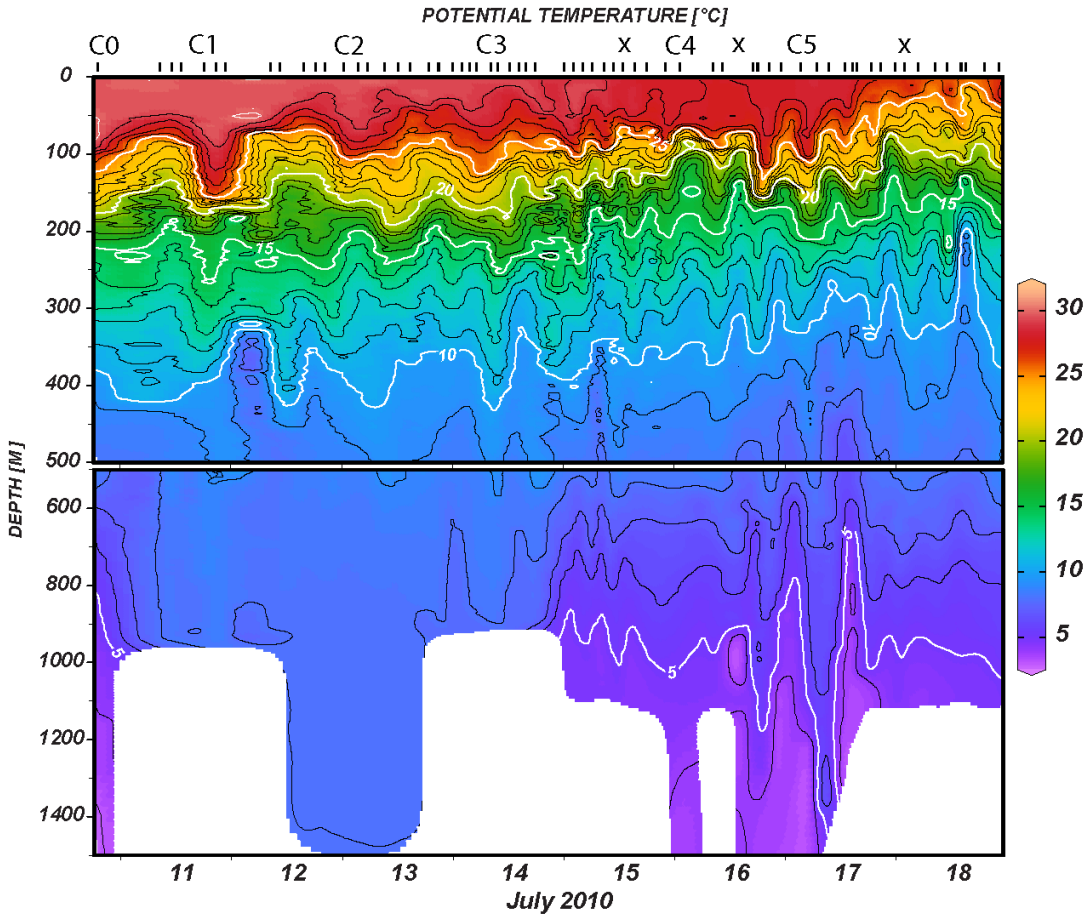

Figure 9. Same as of Fig.8, but for salinity section.

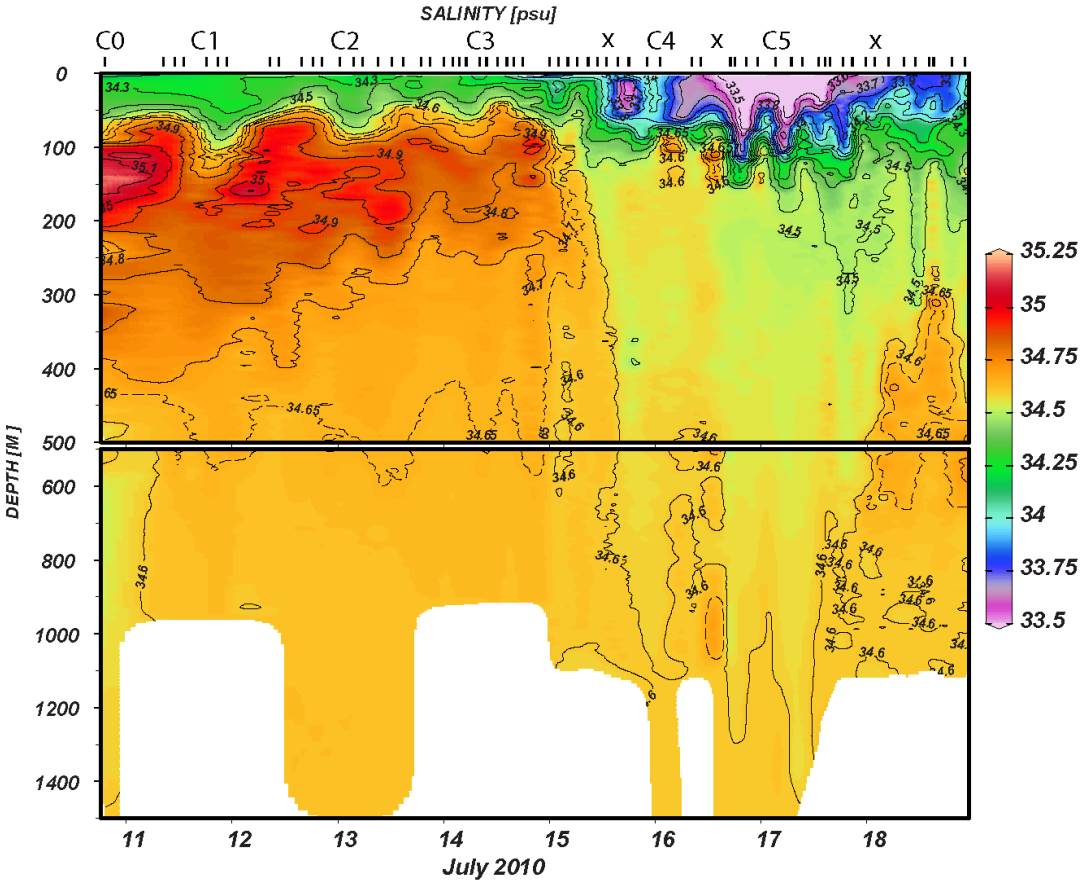

Figure 10. Same as of Fig.8, but for potential density anomaly section. Black dots denote mixed layer depth thickness calculated from each vertical gradient of potential density anomaly, with reference to surface density.

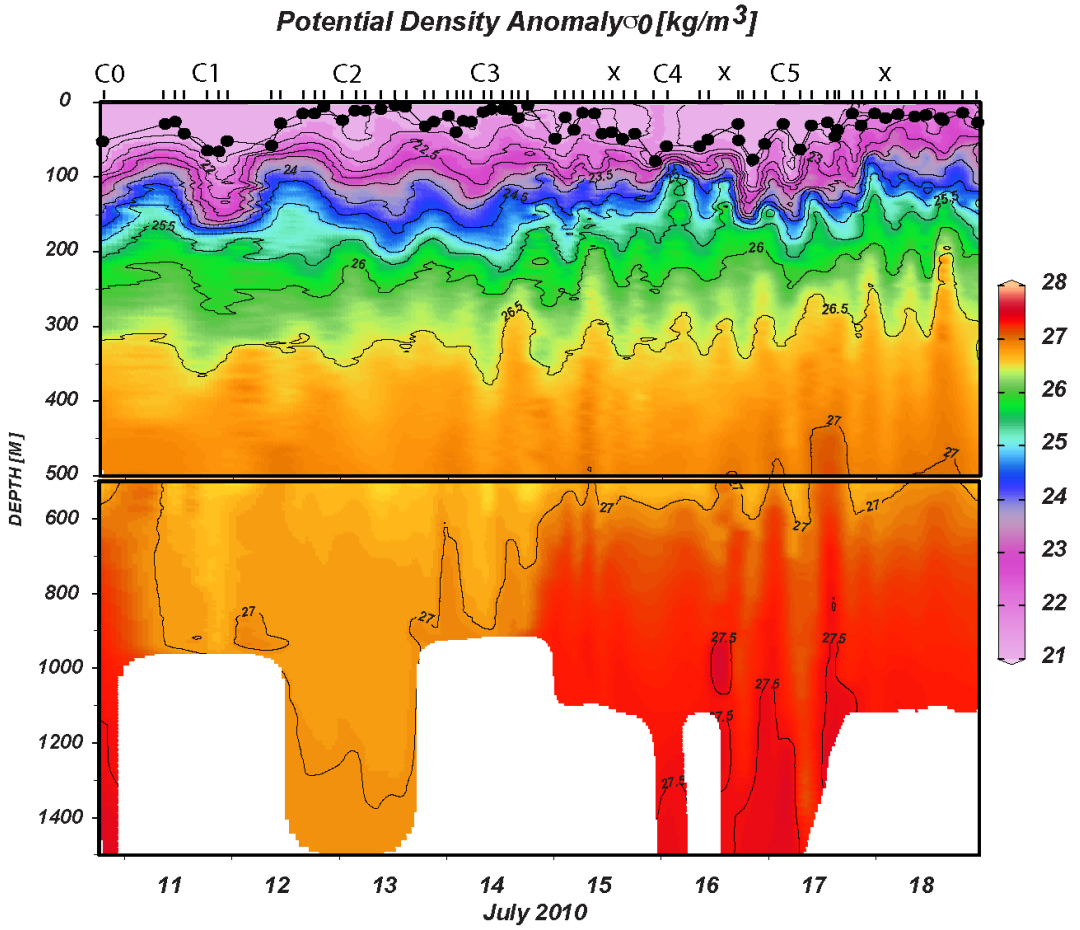

Figure 11. Same as Fig.8, but for dissolved oxygen section.

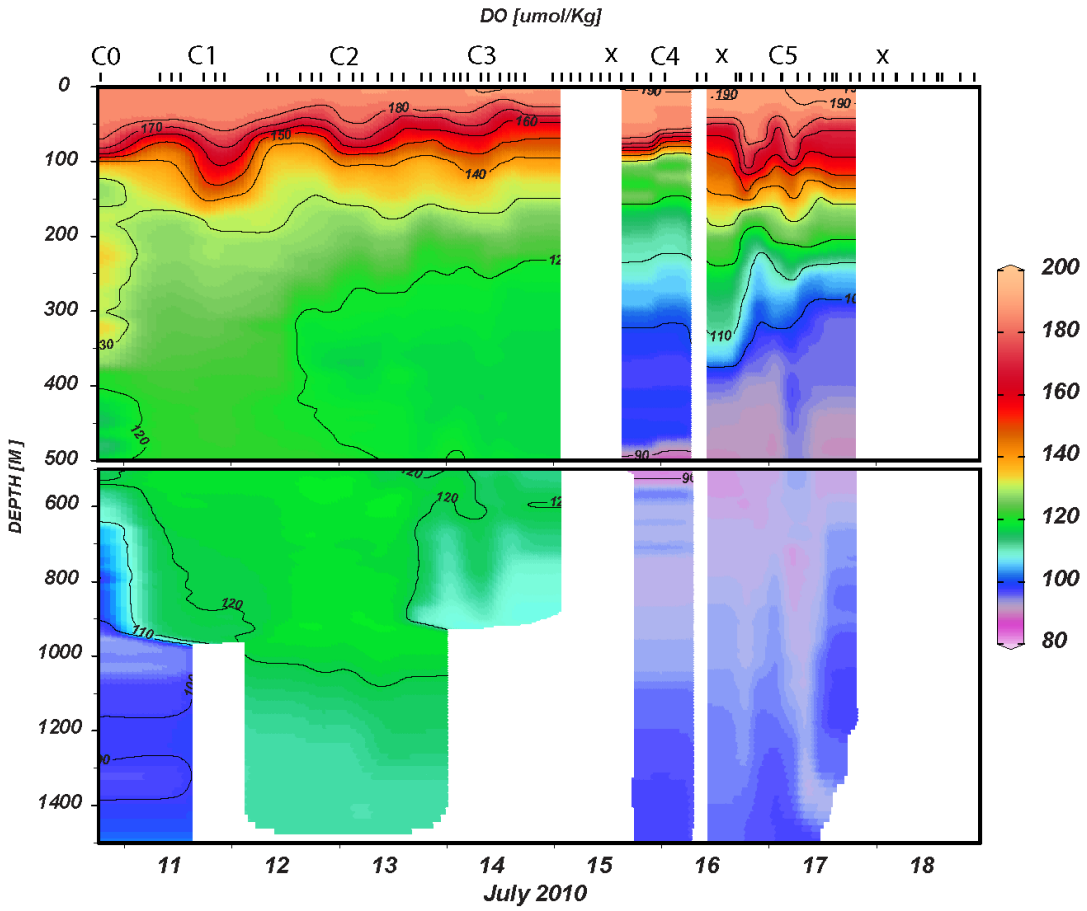

Figure 12. Vertical profiles of temperature (upper panel) and salinity (lower panel) at the entrance of the Halmahera Sea - Pacific station (C0, blue) compared to the mean profile in the Halmahera Sea (average of stations C1, C2, and C3, black line, and thin grey lines correspond to each profile in C1, C2, and C3). Red line is the result of the 1D diffusion model using Kz measured by VMP from INDOMIX and the C0 profile. The first column shows the profile obtained after 0.5 days, second column after 1 day, and third column after 2 days using the Kz1 measured at C1 by the VMP (magenta lines in the right panel). The fourth and fifth columns correspond respectively to 1 day and 2 days after applying the Kz3 value from station C3 (green line in the right panel). Step-like features when applying Kz1 are found due to two maxima in the Kz at 350 m and 600 m depth. After 2 days of Kz1 and 1 day of Kz3 the water mass reached their observed well mixed temperature and salinity profiles.

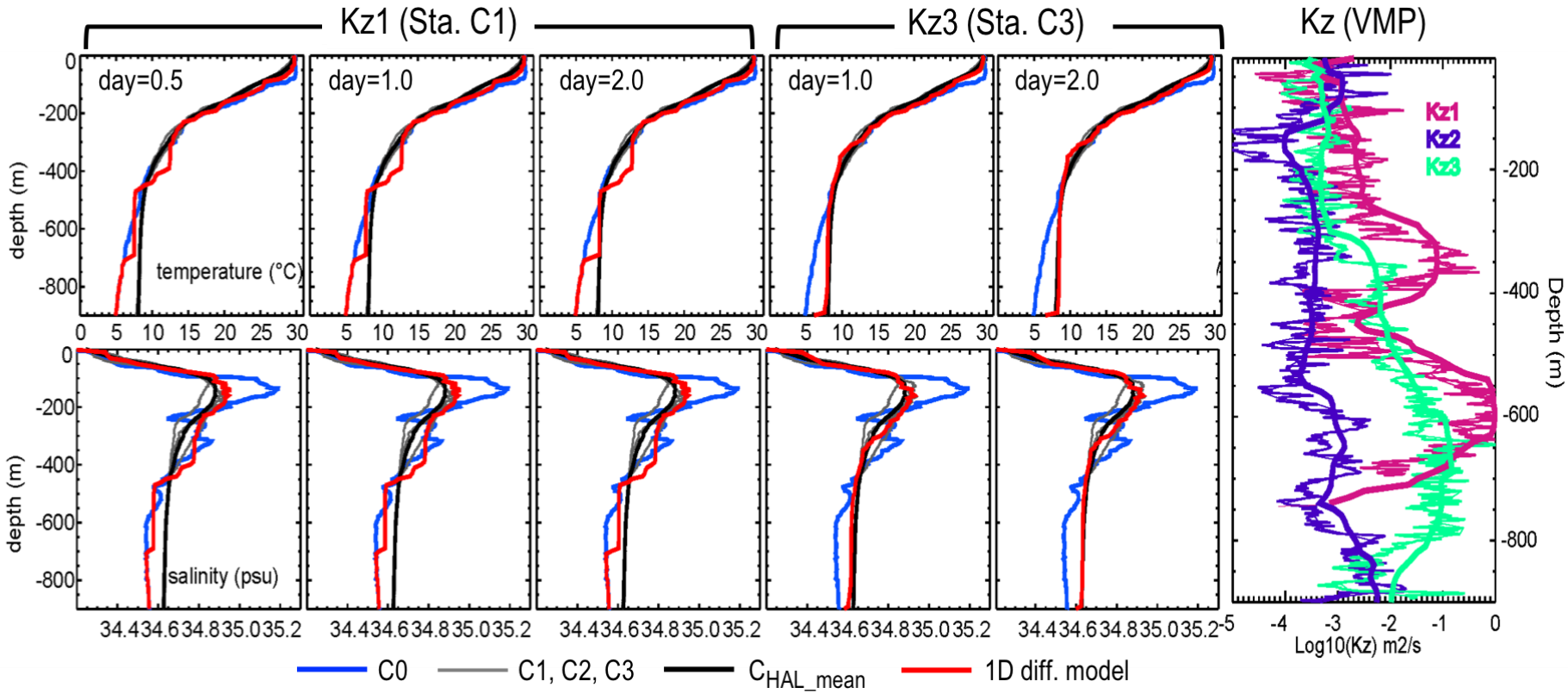
Kz1 (Sta. C1)
Kz3 (Sta. C3)
Kz (VMP)
day=0.5
day=1.0
day=2.0
day=1.0
day=2.0
depth (m)
temperature (°C)
salinity (psu)
Kz1
Kz2
Kz3
Depth (m)
Log10(Kz) m2/s
C0
C1, C2, C3
C_HAL_mean
1D diff. model

10